J. metamorphic Geol., 1995, 13, 397–417

Formation of wollastonite-bearing marbles during late regional metamorphic channelled fluid flow in the Upper Calcsilicate Unit of the Reynolds Range Group, central Australia*

I. CARTWRIGHT[1] AND I. S. BUICK[2]
[1]Victorian Institute of Earth and Planetary Sciences, Department of Earth Sciences, Monash University, Clayton, Vic. 3168, Australia
[2]Victorian Institute of Earth and Planetary Sciences, School of Earth Sciences, LaTrobe University, Bundoora, Vic. 3083, Australia

ABSTRACT Granulite facies marbles from the Upper Calcsilicate Unit of the Reynolds Range, central Australia, contain metre-scale wollastonite-bearing layers formed by infiltration of water-rich ($X_{CO_2} = 0.1–0.3$) fluids close to the peak of regional metamorphism at *c.* 700° C. Within the wollastonite marbles, zones that contain <10% wollastonite alternate on a millimetre scale with zones containing up to 66% wollastonite. Adjacent wollastonite-free marbles contain up to 11% quartz that is uniformly distributed. This suggests that, although some wollastonite formed by the reaction calcite + quartz = wollastonite + CO_2, the wollastonite-rich zones also underwent silica metasomatism. Time-integrated fluid fluxes required to cause silica metasomatism are one to two orders of magnitude higher than those required to hydrate the rocks, implying that time-integrated fluid fluxes varied markedly on a millimetre scale. Interlayered millimetre- to centimetre-thick marls within the wollastonite marbles contain calcite + quartz without wollastonite. These marls were probably not infiltrated by significant volumes of water-rich fluids, providing further evidence of local fluid channelling. Zones dominated by grandite garnet at the margins of the marl layers and marbles in the wollastonite-bearing rocks probably formed by Fe metasomatism, and may record even higher fluid fluxes. The fluid flow also reset stable isotope ratios. The wollastonite marbles have average calcite (Cc) $\delta^{18}O$ values of 15.4 ± 1.6‰ that are lower than the average $\delta^{18}O$(Cc) value of wollastonite-free marbles (*c.* 17.2 ± 1.2‰). $\delta^{13}C$(Cc) values for the wollastonite marbles vary from 0.4‰ to as low as −5.3‰, and correlations between $\delta^{18}O$(Cc) and $\delta^{13}C$(Cc) values probably result from the combination of fluid infiltration and devolatilization. Fluids were probably derived from aluminous pegmatites, and the pattern of mineralogical and stable isotope resetting implies that fluid flow was largely parallel to strike.

Key words: carbon isotopes; central Australia; fluid flow; metasomatism; oxygen isotopes.

Mineral abbreviations and formulae

Carbonate: Cc = Calcite, $CaCO_3$; Dol = Dolomite, $CaMg(CO_3)_2$. Feldspar: Ab = Albite, $NaAlSi_3O_8$; An = Anorthite, $CaAl_2Si_2O_8$; Or = Orthoclase, $KAlSi_3O_8$. Garnet: Al = Almandine, $Fe_3Al_2Si_3O_{12}$; Ad = Andradite, $Ca_3Fe_2Si_3O_{12}$; Gr = Grossular, $Ca_3Al_2Si_3O_{12}$; Py = Pyrope, $Mg_3Al_2Si_3O_{12}$; Sp = Spessartine, $Mn_3Al_2Si_3O_{12}$. Pyroxene: Cats = Ca-Tschermak, $CaAl_2SiO_6$; Di = Diopside, $CaMgSi_2O_6$; Ess = Esseneite, $CaAlFe^{3+}SiO_6$; Hed = Hedenbergite, $CaFeSi_2O_6$. Fo = Forsterite, $MgSi_2O_4$; Mei = Meionite, $Ca_4Al_6Si_6O_{24}CO_3$; Phl = Phlogopite, $KMg_3Si_3Al_2O_{10}(OH)_2$; Qtz = Quartz, SiO_2; Rut = Rutile, TiO_2; Tit = Titanite, $CaTiSiO_5$; Tr = Tremolite, $Ca_2Mg_5Si_8O_{22}(OH)_2$; Woll = Wollastonite, $CaSiO_3$; Zo = Zoisite, $Ca_2Al_3(SiO_4)_3(OH)$. General abbreviations (compositions not specified): Crd = Cordierite; Bt = Biotite; Plg = Plagioclase feldspar; Scap = Scapolite; Sill = Sillimanite.

INTRODUCTION

Constraining fluid–rock interaction during metamorphism is important for the following reasons: (1) the infiltration of large volumes of fluid may cause significant metasomatism, and may lead to the formation of economic mineral deposits; (2) fluid flow may transfer significant quantities of heat (e.g. Norton & Knight, 1977); (3) determining the spatial pattern of fluid flow and time-integrated fluid fluxes helps to constrain crustal-scale hydrogeological regimes; and (4) fluids affect the rheology of the crust and can thus control deformation. The fluid advection–dispersion models that were developed in hydrogeology (e.g. Bear, 1972; deMarsily, 1986) have recently been applied to the study of metamorphic fluid infiltration (e.g. Bickle &

*This paper is a contribution to IGCP project 304, 'Lower Crustal Processes'.

McKenzie, 1987; Ganor *et al.*, 1989; Bickle & Baker, 1990; Cartwright & Valley, 1991; Baumgartner & Ferry, 1991; Ferry & Dipple, 1991, 1992; Dipple & Ferry, 1992; Bowman & Willet, 1992; Cartwright & Weaver, 1993; Todd & Evans, 1993; Cartwright, 1994; Cartwright & Oliver, 1994). These models allow a number of parameters, including time-integrated fluid fluxes, the direction of fluid flow and intrinsic permeabilities, to be calculated from resetting of stable-isotope values, changes in major or trace-element geochemistry, and/or changes in mineral assemblages or the modal amount of minerals. Metacarbonate rocks are ideal for the study of fluid–rock interaction as they readily undergo reaction with incoming fluids to form mineral assemblages that allow fluid compositions to be constrained (e.g. Tracy & Frost, 1991). Additionally, since the initial oxygen isotope ratios of carbonates are generally different from other crustal rocks, fluid infiltration is usually marked by significant isotopic resetting (e.g. Valley *et al.*, 1990; Nabelek, 1991).

In this study, we examine fluid infiltration of water-rich fluids into marbles of the Reynolds Range Group, central Australia, and discuss, in particular: (1) the timing of fluid flow; (2) the spatial pattern of fluid infiltration; (3) variations in time-integrated fluid fluxes and intrinsic permeabilities; and (4) the source of the fluids.

Regional geology

The Reynolds Range (Fig. 1) is a multiply deformed and metamorphosed Proterozoic terrane that forms part of the Arunta Block of central Australia (e.g. Stewart *et al.*, 1980; Black *et al.*, 1983; Warren & Stewart, 1988; Dirks, 1990). The Reynolds Range crops out for over 100 km as a semi-continuous narrow range of rugged hills, and consists of two stratigraphic associations. A suite of pelitic and semipelitic metasediments, the Lander Rock Beds, together with early granitic plutons, form the basement to metasediments of the Reynolds Range Group. The Reynolds Range Group rocks are themselves intruded by later granitic plutons. The main rock types in the Reynolds Range Group are: (1) a 500–600-m-thick basal quartzite; (2) a unit of homogeneous pelitic metasediments with a minimum thickness of 500–600 m; (3) the Lower Calcsilicate Unit that is laterally equivalent to the base of the quartzite unit, and which comprises up to 200 m of siliceous marls with minor lenses of quartzite and marble; and (4) the Upper Calcsilicate Unit that comprises a 300–350-m-thick prominent horizon of generally silicate-poor dolomite- and/or calcite-rich limestones and interlayered calcareous marls (Dirks, 1990). The Upper Calcsilicate Unit is the focus of this study; fluid–rock interaction in the Lower Calcsilicate Unit and the metapelites are discussed by Buick & Cartwright (1994) and Buick *et al.* (1994a).

Tectonometamorphic history of the Reynolds Range

The metamorphic and structural history of the Reynolds Range has been described by Dirks & Wilson (1990), Dirks *et al.* (1991), Clarke *et al.* (1990), Clarke & Powell (1991), Hand *et al.* (1992), Buick *et al.* (1994a) and Vry & Cartwright (1994). In this study the structural and metamorphic terminology of Hand *et al.* (1992) and Buick *et al.* (1994a) is used. An alternative structural–metamorphic framework was proposed by Clarke *et al.* (1990) and Clarke & Powell (1991). The earliest metamorphic–deformation cycle, D1–M1, affected the metasediments of the Lander Rock Beds prior to the

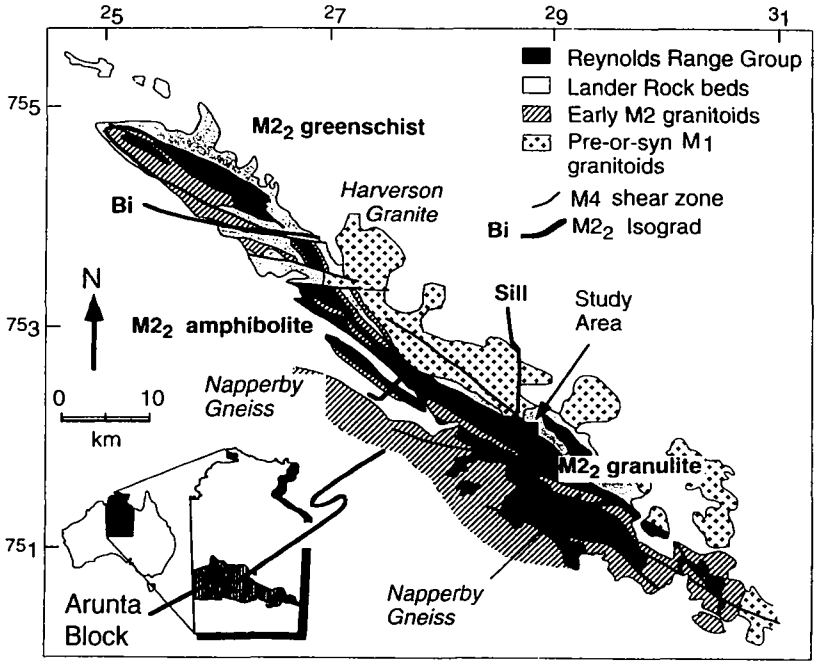

Fig. 1. Simplified geological map of the Reynolds Range, central Australia, showing the major stratigraphic units and $M2_2$ isograds (after Dirks *et al.*, 1991; Buick *et al.*, 1994a). The study area is shown by the solid square.

deposition of the Reynolds Range Group (Clarke *et al.*, 1990; Hand *et al.*, 1992). The main structural–metamorphic event to affect the Reynolds Range Group, D2–M2, involved NE–SW shortening of the range to form tight to isoclinal NW–SE-trending upright isoclinal folds. M2–D2 commenced with the formation of a metamorphic foliation ($S2_1$) that is most commonly preserved as inclusions in porphyroblasts in the contact aureoles of granites intruded before the regional metamorphic peak (Dirks & Wilson, 1990). The development of a penetrative, subvertical NW–SE-trending fabric ($S2_2$) occurred during $D2_2$ deformation synchronous with medium- to low-pressure regional metamorphism ($M2_2$). $M2_2$ ranges in grade from greenschist (*c.* 400° C) in the north-west to granulite (*c.* 740 ± 40° C) in the south-east, at a pressure of 400–500 MPa (Dirks *et al.*, 1991; Vry & Cartwright, 1994). The $M2_2$ isograds, defined by assemblages in Reynolds Range Group metapelites, intersect the strike of the ranges at high angles (Dirks *et al.*, 1991; Fig. 1).

The $D2_2$ structures are locally deformed on regional to outcrop scales by D3 crenulation bands that contain M3 assemblages. The grade of M3 and $M2_2$ assemblages are generally coincident, suggesting that M3 occurred soon after $M2_2$, before the rocks had cooled significantly. The $D2_2$ and D3 structures are disrupted by a system of major NE-dipping D4 thrusts that are interconnected by numerous small shear zones. The grade of M4 assemblages developed during fluid flow within D4 shear zones is lower than, but varies somewhat sympathetically with, the grade of $D2_2$ assemblages, and locally reached mid-amphibolite facies conditions (Dirks *et al.*, 1991). D4 shear zones were locally reactivated during greenschist facies shearing of Permo-Carboniferous age during the Alice Springs Orogeny (Dirks & Wilson, 1990). In this paper we describe fluid–rock interaction in the Upper Calcsilicate Unit that occurred during the latter stages of the $D2_2$–$M2_2$ tectonometamorphic cycle.

ANALYTICAL TECHNIQUES

Mineral compositions were determined on the Cameca Camebax SX50 electron microprobe at the University of Melbourne (15 kV, 25 nA) using wavelength-dispersive spectrometry. Routine analyses were made for the elements S, P, Na, Mg, Al, Fe, Si, K, Ti, Cr, Mn, Ca, Cl and F, and data were reduced using PAP corrections provided by the manufacturer. Iron was analysed as FeO, and Fe_2O_3 in pyroxenes and garnets was calculated using crystal chemical and stoichiometric constraints. Stable isotope ratios were measured at Monash University. Analyses of carbonate-rich samples were performed on mixed carbonate/silicate powders extracted by a dentist's drill, and thus represent samples of *c.* 1–3 mm^3. Although efforts were made to sample the different mineralogical zones in the rocks (described below), the complex geometry and small size of the zones made this difficult. Mineral separates were hand picked from cubes of rock (*c.* 1 cm on a side) that had been coarsely crushed, sieved and treated with HCl to remove any carbonate. Oxygen isotope ratios of silicates were analysed following Clayton & Mayeda (1963) using ClF_3 as the oxidizing reagent, and CO_2 was extracted from calcite by reaction with H_3PO_4 at 25° C for 12–18 h in sealed vessels (McCrea, 1950). The extracted gases were analysed as CO_2 on Finnigan MAT Delta-E and 252 mass spectrometers and the results are expressed relative to PDB (carbon) and V-SMOW (oxygen). Internal and international standards run at the same time as the samples from this study generally yielded values within ±0.2‰ of their accepted values.

FIELD RELATIONS

The mineral assemblages and modes of the carbonate rocks in the study area are summarized in Table 1, and representative mineral analyses presented in Table 2. The Upper Calcsilicate Unit of the Reynolds Range Group contains two main rock types. The majority of the unit consists of *marbles* that may be subdivided into calcite + diopside + quartz + K-feldspar-bearing 'calcite marbles' and calcite + dolomite + forsterite + spinel-bearing 'dolomite marbles'. These two marble types are interlayered parallel to stratigraphy on a metre to hundreds of metre scale and probably represent protoliths with different initial compositions. Within both types of marbles are concordant, millimetre- to centimetre-wide, fine-grained bands and lenses that contain less carbonate

Table 1. Modal mineralogy of marbles from the Upper Calcsilicate Unit.

	Modal mineralogy*					
Sample	Cc	Qtz	Di	An	Or	Phl
Calcite marbles						
9235-136	68 (18)†	11 (4.8)	14	6	1	0
9235-137	70 (19)	10 (4.4)	11	3	6	0
9235-138	68 (18)	9 (4.0)	14	7	0	2
9235-139	76 (21)	7 (3.1)	5	8	4	0
9235-140	75 (20)	9 (4.0)	7	6	3	0
9235-141	74 (20)	8 (3.5)	8	5	0	5
9235-142	76 (21)	7 (3.1)	7	6	4	0
9235-143	72 (19)	6 (2.6)	11	7	4	0
9235-145	73 (20)	6 (2.6)	13	4	4	0
9235-147	72 (19)	8 (3.5)	6	5	0	9
9235-148	80 (22)	7 (3.1)	8	4	0	1
Average	73	8	9	6	1	3

	Modal mineralogy*						
Sample	Cc	Qtz	Di	An	Or	Woll	Gr
Wollastonite marbles							
9235-119R‡	72	7	6	4	5	1 (0.3)†	5
9235-119wp‡	10	1	9	4	3	61 (15)	12
9235-122	61	5	16	7	4	3 (0.8)	4
9235-123	19	2	6	2	2	55 (14)	14
9235-124	12	2	5	3	1	66 (17)	11
9235-125	10	1	6	4	2	65 (16)	12
9235-127	24	1	13	7	6	40 (10)	9
9235-128R	63	7	11	5	4	3 (0.8)	7
9235-128wp	12	1	9	5	5	58 (15)	10
9235-130R	71	4	8	6	1	1 (0.3)	9
9235-130wp	15	2	6	12	7	50 (13)	8
9235-362R	62	6	12	7	2	3 (0.8)	8
9235-363R	72	7	7	4	3	2 (0.6)	5
9235-363wp	22	1	10	3	2	55 (14)	7
9235-366	14	1	8	11	4	56 (14)	6
9235-368a	12	1	12	4	3	59 (15)	9
9235-369	68	5	11	3	2	7 (1.8)	4
9235-370R	67	6	9	5	3	2 (0.6)	8
9235-370wp	17	1	11	2	4	54 (13)	11

*Modal mineralogy estimated by point counting (typically 1000 points); †$mol/m^3 \times 10^{-3}$; ‡WR, wp = wollastonite-rich and wollastonite-poor zones.

Table 2a. Clinopyroxene compositions from calcite and wollastonite marbles.

	Calcite marbles			Wollastonite marbles											
Sample	147 Mbl (C)	147 Mbl (R)	140 Mbl (R)	362 Mbl (C)	362 Mbl (R)	362 GZ (C)	362 GZ (R)	363 GZ (R)	363 Mbl (C)	363 Mbl (R)	363 Marl (C)	363 GZ (C)	368 Mbl (C)	368 GZ (C)	386 Marl (C)
SiO_2	54.15	54.46	51.06	52.73	53.06	53.62	53.02	53.34	52.75	53.34	53.09	52.75	52.62	52.87	51.45
TiO_2	0.07	0.04	0.03	0.01	0.03	0.03	0.04	0.04	0.04	0.02	0.05	0.04	0.06	0.02	0.01
Al_2O_3	0.60	0.40	1.21	0.82	1.21	0.89	0.71	0.68	1.28	0.79	1.19	1.28	0.96	0.43	0.70
Cr_2O_3	0.00	0.00	0.01	0.05	0.01	0.00	0.04	0.00	0.03	0.04	0.01	0.03	0.00	0.02	0.10
Fe_2O_3	0.47	0.32	1.68	1.94	1.68	0.35	0.52	0.36	0.31	0.00	0.00	0.31	0.00	0.63	2.11
MgO	17.14	17.41	13.76	14.41	13.76	13.90	14.30	14.68	13.76	14.09	13.65	13.76	13.87	14.17	12.90
CaO	25.58	25.48	25.02	25.66	25.06	25.42	25.54	25.70	25.71	25.75	25.54	25.71	24.70	25.45	25.16
MnO	0.09	0.06	0.35	0.41	0.35	0.46	0.44	0.40	0.41	0.42	0.32	0.41	0.06	0.26	0.21
FeO	1.19	1.24	3.79	2.60	3.79	5.00	4.39	4.00	4.89	4.62	5.42	4.89	6.57	5.15	5.57
Na_2O	0.04	0.03	0.07	0.05	0.07	0.03	0.05	0.05	0.06	0.05	0.04	0.06	0.07	0.05	0.09
Total	99.33	99.44	96.99	98.68	99.03	99.69	99.06	99.25	99.24	99.11	99.31	99.24	98.91	99.06	98.31
Cations per 6 oxygens															
Si	1.98	1.99	1.95	1.98	1.98	1.98	1.98	1.98	1.97	1.99	1.98	1.97	1.99	1.98	1.96
Ti	0.00	0.00	0.00	0.00	0.00	0.00	0.00	0.00	0.00	0.00	0.00	0.00	0.00	0.00	0.00
Al	0.03	0.02	0.06	0.04	0.05	0.04	0.03	0.03	0.06	0.04	0.05	0.06	0.04	0.02	0.03
Cr	0.00	0.00	0.00	0.00	0.00	0.00	0.00	0.00	0.00	0.00	0.00	0.01	0.00	0.00	0.00
Fe^{3+}	0.01	0.01	0.05	0.06	0.04	0.01	0.02	0.01	0.01	0.00	0.00	0.01	0.00	0.02	0.06
Mg	0.94	0.95	0.78	0.81	0.78	0.78	0.80	0.81	0.77	0.79	0.76	0.77	0.78	0.80	0.73
Ca	1.00	0.99	1.02	1.01	1.01	1.02	1.02	1.02	1.03	1.03	1.02	1.02	0.97	1.01	1.03
Mn	0.00	0.00	0.01	0.01	0.01	0.02	0.01	0.01	0.01	0.01	0.01	0.01	0.00	0.01	0.01
Fe^{2+}	0.04	0.04	0.12	0.08	0.12	0.16	0.14	0.12	0.15	0.15	0.17	0.15	0.21	0.16	0.18
Na	0.00	0.00	0.01	0.00	0.01	0.00	0.00	0.00	0.00	0.03	0.03	0.00	0.01	0.00	0.01
Di	92.6	92.4	79.8	84.2	80.0	80.9	83.0	85.1	80.2	83.6	79.0	80.2	73.4	80.7	75.1
Ess	1.3	0.9	4.8	5.6	3.8	1.0	1.5	1.0	0.9	0.0	0.0	0.9	0.0	1.8	6.0
CaTs	0.6	0.5	0.6	1.3	2.7	1.5	1.3	1.3	2.7	2.5	3.5	2.7	3.0	0.4	-1.0
Woll	49.6	49.3	49.9	50.4	50.0	50.5	50.5	50.7	50.6	51.1	50.6	50.6	48.3	50.0	50.2
Hed	3.6	4.1	12.3	8.5	12.4	16.3	14.3	13.0	16.0	15.5	17.5	16.0	19.5	16.4	18.2

Sample numbers preceeded by 9235; (C) = core (R) = rim.

Table 2b. Garnet compositions from wollastonite marbles.

Sample	127 Mbl*	127 Mbl†	127 Mbl (R)	127 Mbl (C)	362 Mbl*	362 Mbl‡	362 GZ	362 Mbl†	362 Mbl*	362 GZ§	362 GZ¶	368A Mbl	368A GZ§	368A GZ¶	386A Vein
SiO_2	38.92	38.71	37.38	36.32	37.97	36.75	36.61	37.89	38.72	36.85	37.17	38.82	36.26	37.95	36.86
TiO_2	0.60	0.20	0.43	0.65	0.33	0.20	0.52	0.21	0.46	0.67	0.62	0.01	0.40	0.16	0.02
Al_2O_3	18.00	17.76	14.67	9.57	16.78	17.33	9.59	16.75	16.55	7.46	9.82	21.39	6.16	19.60	9.94
Cr_2O_3	0.00	0.00	0.02	0.00	0.02	1.72	0.04	0.00	0.01	0.11	0.06	0.03	0.00	0.03	0.00
Fe_2O_3	5.50	6.59	10.33	17.21	7.76	5.09	17.34	7.83	8.08	19.68	16.91	1.75	22.39	3.78	17.63
MgO	0.00	0.00	0.00	0.00	0.00	0.00	0.00	0.00	0.00	0.00	0.00	0.00	0.00	0.00	0.00
CaO	36.40	36.36	35.77	34.60	36.34	36.58	34.88	36.14	36.45	33.23	34.12	37.62	33.93	36.65	35.29
MnO	0.47	0.39	0.33	0.17	0.40	0.30	0.20	0.35	0.39	0.49	0.25	0.21	0.19	0.25	0.16
FeO	0.00	0.16	0.16	0.66	0.44	1.30	0.13	0.51	0.00	0.84	0.53	0.42	0.53	0.85	0.25
ZnO	0.00	0.00	0.10	0.10	0.06	0.00	0.06	0.05	0.00	0.00	0.00	0.00	0.00	0.13	0.00
Total	99.89	100.16	99.20	99.28	100.11	99.28	99.37	99.72	100.66	99.33	99.47	100.24	99.86	99.39	100.16
Cations per 12 oxygens															
Si	2.99	2.986	2.95	2.94	2.95	2.89	2.97	2.98	2.98	2.97	3.00	2.94	2.97	2.93	2.96
Ti	0.04	0.01	0.03	0.04	0.02	0.01	0.03	0.01	0.03	0.04	0.03	0.00	0.03	0.01	0.00
Al	1.63	1.60	1.37	0.91	1.52	1.55	0.92	1.52	1.50	0.73	0.93	1.91	0.60	1.77	0.94
Cr	0.00	0.00	0.01	0.00	0.00	0.11	0.00	0.00	0.00	0.01	0.00	0.00	0.00	0.00	0.00
Fe^{3+}	0.32	0.38	0.61	1.05	0.45	0.30	1.06	0.45	0.47	1.22	1.03	0.10	1.38	0.22	1.07
Mg	0.00	0.00	0.00	0.00	0.00	0.00	0.00	0.00	0.00	0.00	0.00	0.00	0.00	0.00	0.00
Ca	3.00	3.00	3.00	3.00	3.00	3.03	3.00	2.98	3.00	2.95	2.96	3.01	2.98	3.00	3.01
Mn	0.03	0.03	0.02	0.01	0.03	0.02	0.01	0.02	0.03	0.03	0.02	0.01	0.01	0.02	0.01
Fe^{2+}	0.00	0.01	0.01	0.04	0.03	0.09	0.01	0.03	0.00	0.06	0.02	0.03	0.04	0.05	0.02
Zn	0.00	0.00	0.01	0.01	0.00	0.00	0.04	0.03	0.00	0.00	0.00	0.00	0.00	0.01	0.000
Gr	81.1	79.2	67.3	44.4	74.7	75.6	45.3	75.1	74.5	35.3	46.1	93.9	29.2	86.5	46.4
Ad	15.8	18.9	30.2	51.6	22.3	14.6	52.2	22.3	23.2	59.1	50.7	4.9	67.9	10.7	52.7
Al	0.0	0.3	0.2	0.7	0.7	2.1	0.1	0.7	0.0	0.7	0.4	0.8	0.4	1.3	0.3
Py	0.0	0.0	0.0	0.0	0.0	0.0	0.0	0.0	0.0	0.0	0.0	0.0	0.0	0.0	0.0
Sp	0.8	0.7	0.5	0.2	0.7	0.5	0.2	0.5	0.6	0.4	0.3	0.4	0.1	0.5	0.2

Sample numbers preceeded by 9235; (C) = core (R) = rim. *Low woll zone; †high woll zone; ‡rim on scapolite; §highest X_{Ad}; ¶lowest X_{Ad}.

and probably represent *marl* layers. Locally, the marl layers and the marbles are separated by discontinuous millimetre- to centimetre-wide rims of diopside or plagioclase that is of similar composition to the minerals of the marl layers (Table 2). The rims are present in rocks from the upper amphibolite to granulite facies portions of the Upper Calcsilicate, and where the marl layers are boudinaged parallel to $S2_2$ the rims usually follow the outlines of the boudins. In this portion of the Reynolds Range, the Upper Calcsilicate Unit is surrounded by metapelites (Fig. 1).

Throughout the Upper Calcsilicate Unit, wollastonite marbles occur as strike-parallel layers within both the dolomite and the calcite marbles. These layers may be up to tens of metres wide and hundreds of metres long and have relatively sharp margins with the surrounding

Table 2c. Plagioclase compositions from calcite and wollastonite marbles.

	Calcite marble			Wollastonite marble	
Sample	127 Mbl	127 Marl*	127 Marl	362 Mblt	362 Mbl
SiO_2	43.96	43.75	43.95	42.98	44.46
TiO_2	0.01	0.01	0.00	0.00	0.04
Al_2O_3	36.12	36.07	36.23	35.26	33.66
CaO	20.09	20.07	19.94	20.11	19.98
FeO	0.15	0.25	0.07	0.11	0.05
Na_2O	0.18	0.23	0.12	0.13	0.36
K_2O	0.04	0.03	0.02	0.05	0.17
Total	100.54	100.41	100.34	98.64	98.74
Cations per 8 oxygens					
Si	2.03	2.03	2.03	2.03	2.10
Ti	0.00	0.00	0.00	0.00	0.00
Al	1.96	1.96	1.97	1.96	1.90
Ca	0.99	0.98	0.99	0.99	0.96
Fe	0.01	0.01	0.00	0.00	0.00
Na	0.02	0.02	0.01	0.01	0.03
K	0.00	0.00	0.00	0.00	0.01
An	99	98	99	99	96
Ab	1	2	1	1	3
Or	0	0	0	0	1

Sample numbers preceeded by 9235. *Edge of marl layer; †after scapolite.

Table 2d. Mineral compositions in dolomite marble.

Sample	146 Phl	146 Fo
SiO_2	39.843	40.19
TiO_2	0.57	0.00
Al_2O_3	15.92	46.90
MgO	24.52	0.05
CaO	0.02	0.18
MnO	0.04	13.53
FeO	3.27	0.00
Na_2O	0.17	0.00
K_2O	10.56	0.00
F	1.18	
Cl	0.08	
O = F	−0.50	
O = Cl	−0.02	
Total	95.65	100.86
Si	6.10	0.99
Ti	0.07	0.00
Al	2.87	0.00
Mg	5.59	1.73
Ca	0.00	0.00
Mn	0.01	0.00
Fe2 +	0.42	0.28
Na	0.05	0.00
K	2.06	0.00
	Phl = 39.8;	Fo = 74.0.

Sample numbers preceeded by 9235.

wollastonite-free marbles. Centimetre- to decimetre-scale lenses of wollastonite-free marble that are orientated parallel to $S2_2$ occur within the wollastonite marbles. Marl layers are recognizable in the wollastonite marbles, and, in place of the diopside or plagioclase, a millimetre- to centimetre-wide zone dominated by grandite garnet with minor (<10%) calcite generally separates the marble and marl layers. At high $M2_2$ grades the total across-strike distance of wollastonite marble varies from less than a few metres to hundreds of metres (Fig. 2). Metre- to tens-of-metre thick concordant metapsammite layers that occur within the Upper Calcsilicate locally contain orthoamphibole that, from textural considerations, is inferred to have grown during the later stages of $M2_2$. Thin wollastonite marbles are commonly interlayered with these orthoamphibole layers, suggesting that the wollastonite marbles and orthoamphibole-bearing metapsammite rocks were formed at a similar time. Aluminous pegmatites that cross-cut the $D2_2$ fabrics are common in the Upper Calcsilicate; these bodies are typically a few metres to tens of metres wide and may account for up to 1–2% of the outcrop at high grades. From the relationships with tectonic fabrics, these pegmatites appear to have been emplaced at or later than the peak of the $M2_2$ regional metamorphism. As discussed below, it is likely that the fluid flow in the wollastonite marbles was related to pegmatite emplacement. Macroscopic veins are not abundant in the area; however, millimetre-scale quartz + garnet veins cut both the marble and marl layers within the wollastonite zones. Epidote is commonly formed within a few millimetres of these veins. Additionally, quartz + garnet assemblages occasionally occur in boudin necks within the marls that are orientated parallel to $D2_2$ stretching directions.

In this study we describe samples from a composite traverse across one 40–45-m-wide wollastonite marble layer into the surrounding dominantly calcite marbles, together with wollastonite-bearing and wollastonite-free samples from elsewhere in the Upper Calcsilicate Unit (Figs 1 and 2). The wollastonite marble layer is orientated parallel to $S2_2$ and has relatively sharp margins (to within a few centimetres) with the surrounding marbles. Thin (up to 5 m wide) siliceous layers of cordierite gneiss that are also orientated parallel to $S2_2$ are present within the wollastonite marble (Fig. 2).

PETROLOGY AND MINERAL CHEMISTRY

Calcite and dolomite marbles

The calcite marbles contain 60–90% calcite ($Cc_{0.99}$) together with varying proportions of diopside ($Di_{0.88-0.92}$), alkali feldspar ($Or_{0.99}$), phlogopite (Mg/(Mg + Fe) = 0.93–0.95 with *c.* 1 wt% F, titanite, and 5–15% quartz (Tables 1 and 2). The calcite marbles have granoblastic textures, except for samples 9235-135 and 9235-136 that occur approximately 20 m from the wollastonite marbles which contain moderately strained calcite. The granoblastic textures indicate that the minerals approached textural and chemical equilibrium. Apart from the marl layers, there is little internal layering within these rocks; in particular, no quartz-rich zones are observed, which, as discussed below, places constraints on the wollastonite-forming reactions. The one dolomite marble sample (9235-146) has a granoblastic texture and contains 72% calcite ($Cc_{0.99}$), with dolomite, diopside ($Di_{0.88-0.92}$), phlogopite (Mg/(Mg + Fe) = 0.94), alkali feldspar ($Or_{0.99}$), and forsterite ($Fo_{0.74}$).

Wollastonite marbles

The wollastonite marbles contain up to 66% wollastonite, 5–65% calcite, 2–12% plagioclase, 5–13% diopside, 4–14% garnet, 1–7% K-feldspar and up to 9% quartz in

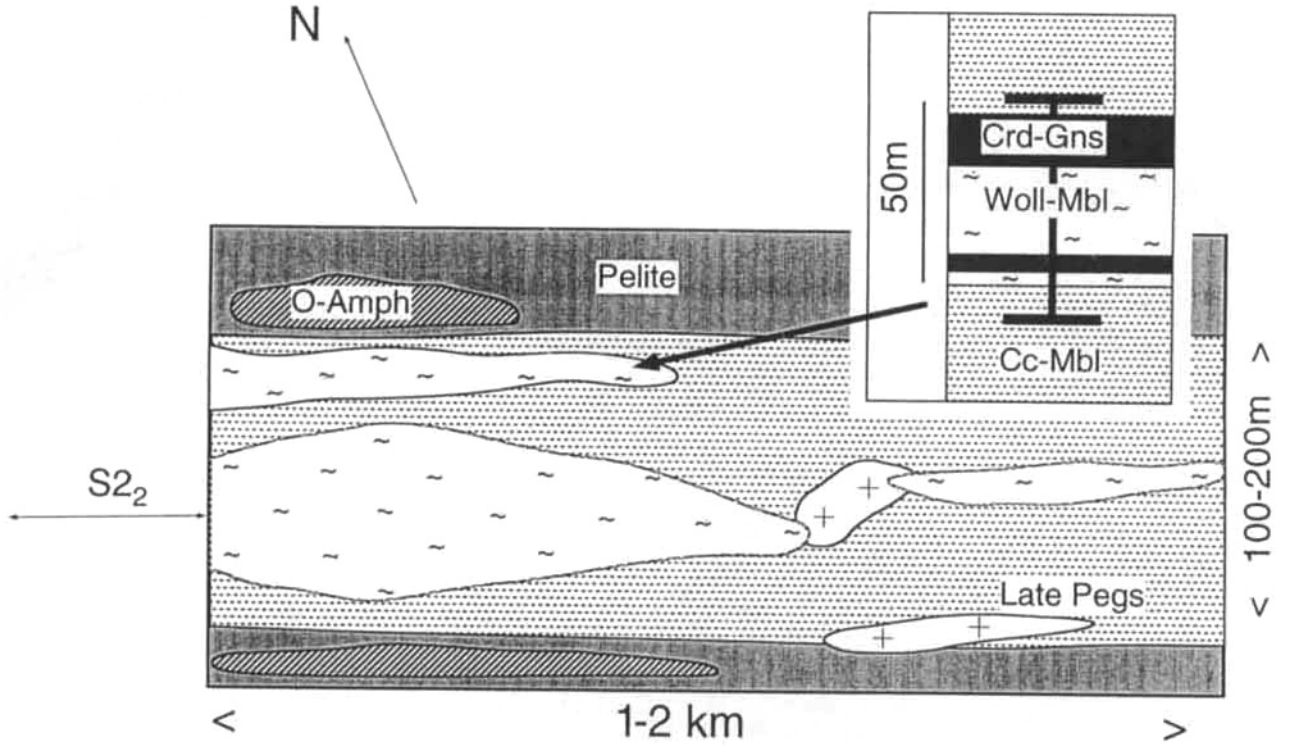

Fig. 2. Cartoon of the Upper Calcsilicate outcrop from the granulite facies region of the Reynolds Range. Wollastonite marbles (Woll-Mbl) occur as approximately concordant layers within calcite marbles (Cc-Mbl) that vary in width along strike. The adjacent pelites locally contain concordant lensoid orthoamphibole-bearing layers (O-Amph) that are also approximately concordant to strike. Aluminous pegmatites cross-cut the $S2_2$ tectonic fabrics defined by the peak $M2_2$ metamorphic minerals, and are interpreted as being emplaced soon after the peak of $M2_2$ metamorphism. Inset: the stratigraphy of the rocks from this study.

samples with lower wollastonite contents (Tables 1 and 2). Wollastonite is virtually pure, with very minor Mn or Fe contents. Most commonly wollastonite occurs as coarse unaligned mats that cut $S2_2$, although wollastonite is locally aligned in $S2_2$. On the scale of an individual thin section there is great variability in the percentage of wollastonite (Table 1; Fig. 3). Quartz-free zones dominated by wollastonite alternate on a millimetre to centimetre scale with zones that contain 50–60% calcite and <10% wollastonite, which are still quartz bearing. The boundaries between the wollastonite-rich and wollastonite-poor zones are usually sharp, and the wollastonite-rich zones are found throughout the wollastonite marbles, including at the margin with the calcite marbles. Clinopyroxene occurs throughout the wollastonite marbles, and is generally diopside rich ($Di_{0.70-0.85}$) with minor hedenbergite ($Hed_{0.04-0.16}$) and esseneite ($Ess_{0-0.06}$) components. Clinopyroxene in the wollastonite marbles has slightly lower Di contents than that in the calcite marbles ($Di_{0.88-0.92}$), and clinopyroxene rims are generally slightly more diopsidic than the cores (Table 2). K-feldspar ($Or_{0.99}$) occurs throughout the wollastonite marbles. Symplectites of plagioclase ($An_{0.97-0.99}$) with calcite and quartz inclusions most probably replace scapolite (Fig. 3c), which locally is common in the Upper Calcsilicate rocks at lower metamorphic grades (Buick & Cartwright, 1994), although no residual scapolite is seen. Plagioclase of similar composition to that in the pseudomorphs occurs sporadically throughout the wollastonite marble, usually rimmed by garnet (see below). Garnet of several distinct compositions, timing and associations may be present in single samples. In some wollastonite-poor areas, skeletal grossular-rich garnet ($Gr_{0.73-0.76}$, $Ad_{0.23-0.25}$) occurs around calcite–quartz or calcite–plagioclase grain boundaries (Fig. 3a). In other areas, slightly more grossular-rich garnet ($Gr_{0.80-0.94}$, $Ad_{0.16-0.05}$) separates wollastonite and calcite or wollastonite and plagioclase. As discussed below, these two generations of skeletal garnet are inferred to have been formed by different mineral reactions. A garnet rim ($Gr_{0.70-0.77}$) also separates the pseudomorphed scapolite from adjacent matrix calcite (Fig. 3c), but no instances of grossular separating the plagioclase and calcite within the symplectite have been noted. Within individual samples, garnet around the pseudomorphed scapolite is of similar composition to that in other parts of the thin section (Table 2). The wollastonite marbles were examined using cathodoluminescence (Fig. 3d). Both the wollastonite-rich and wollastonite-poor zones show little internal variation in luminescence. In particular, there are no indications of vein-type structures, such as have been noted in other studies of marbles from fluid flow zones (e.g. Yardley & Lloyd, 1989; Cartwright & Weaver, 1993).

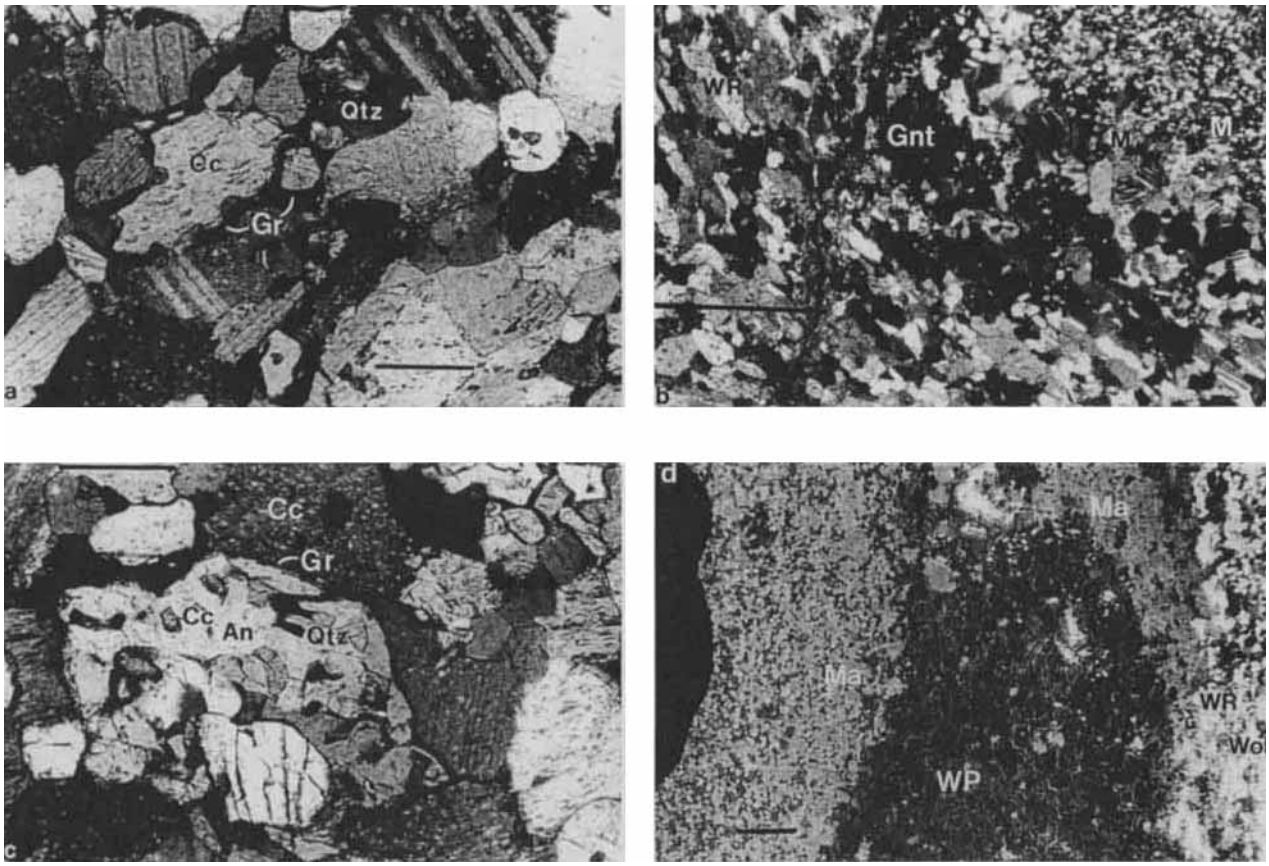

Fig. 3. Photomicrographs of the wollastonite marbles. (a) Grossular (Gr) growing along the grain boundaries between calcite (Cc), and quartz (Qtz) in wollastonite-poor zone. Scale bar = 1 mm. (b) Contact between marl (M) and wollastonite-rich marble (WR) separated by a zone rich in grandite garnet (Gnt). The marls contain calcite + quartz with no wollastonite, whereas the marble adjacent to the grandite-rich zone contains abundant wollastonite. Scale bar = 5 mm. (c) Early scapolite now pseudomorphed by anorthite (An) with inclusions of calcite (Cc) and quartz (Qtz); a thin rim of grossular (Gr) separates this pseudomorph from the surrounding calcite. Scale bar = 1 mm. (d) Wollastonite marble in cathodoluminescence. Wollastonite (Woll) luminesces very brightly, making the contrast between wollastonite-rich (WR) and wollastonite-poor (WP) zones very clear. The marl layer (Ma) contains no wollastonite. Scale bar = 5 mm.

Grandite-rich zones

These zones are restricted to the wollastonite marbles, and are dominated by grandite garnet ($Gr_{0.29-0.46}$, $Ad_{0.53-0.67}$) that overgrows wollastonite in the marbles (Fig. 3b), suggesting that the development of the zone postdated, or outlasted, the formation of wollastonite in the marbles. Although the molar fractions of grossular and andradite may vary across the garnets in the zone, there is no systematic compositional zoning. However, within some samples (e.g. 9235-368A and 9235-167) are zones of anomalously high calcic garnet (up to Gr_{87}) that possibly represent relics of early grossular garnet within the wollastonite marbles that were subsequently overprinted by the more andraditic garnet. In addition, calcite ($Cc_{0.99}$) occurs within these layers, together with clinopyroxene, that, in individual samples, is of similar composition to clinopyroxene in the wollastonite marbles (Table 2). Small (<0.1 mm wide) late veins cut the wollastonite marbles and the grandite-rich zones in some samples. These veins comprise calcite, garnet that is similar in composition to that in the grandite-rich zones (Table 2), and locally epidote.

Marls

The marl layers within the calcite and the wollastonite marbles comprise quartz, calcite, clinopyroxene ($Di_{0.80-0.85}$), plagioclase ($An_{0.94-0.96}$) and K-feldspar ($Or_{0.99}$) with minor titanite (Tables 1 and 2). Some marls in the calcite marbles are also dolomite bearing which, as discussed below, constrains fluid–rock interaction in these rocks. There is little difference in mineral assemblage between the marls in the calcite marbles and those in the wollastonite marbles, and both contain calcite and quartz with no wollastonite. However, the marls in the wollastonite marbles are considerably coarser grained (up to 0.5 mm) than those in the calcite marbles (<0.1 mm). Late epidote is present in a few marls. Cathodluminescence confirmed the lack of wollastonite in the marls as wollastonite luminesces very brightly (Fig. 3d) and even small amounts are readily visible.

Cordierite gneisses

The cordierite gneisses typically comprise cordierite + sillimanite + K-feldspar + tourmaline + magnetite + plagioclase + biotite ±corundum assemblages. They are generally medium grained (1–2 mm diameter) and have millimetre-scale compositional layering defined by alternating cordierite- and sillimanite-rich layers. The sillimanite is generally fibrous, usually defines the $L2_2$ elongation lineation and is locally enveloped by cordierite. Coarse-grained prismatic sillimanite is locally intergrown with the cordierite in blocky aggregates and may be later than the fibrous sillimanite. Because these rocks are interlayered concordantly with the marbles, we interpret them as being metasediments. Their high concentration of aluminous minerals and the lack of free quartz suggests that they may be metamorphosed clays.

Aluminous pegmatites

These rocks occur as metre-scale segregations and veins that locally cross-cut layering and the $S2_2$ fabrics. They are typically composed of coarse-grained (up to 1–2 cm diameter) unaligned minerals. The earliest recognizable mineral assemblage is quartz + sillimanite + cordierite + biotite, together with plagioclase, K-feldspar, monazite, zircon, apatite and tourmaline in some samples. The cordierite typically occurs as subhedral tabular grains and is locally partially altered to a fine-grained aggregate of green biotite + chlorite + andalusite. Because of their relationships to the tectonic fabrics, we interpret these aluminous rocks as being crystallized aluminous melts of the pelites of the Reynolds Range Group and suggest that they formed and were emplaced during the regional $M2_2$ granulite facies metamorphism.

EXTENT AND CONDITIONS OF METAMORPHIC FLUID FLOW

The mineral assemblages in the marble and marl layers allow the conditions of metamorphic fluid flow to be constrained. Figure 4(a) is a T–X_{CO_2} section in the system K_2O–CaO–MgO–Al_2O_3–SiO_2–H_2O–CO_2 (KCMAS) at $P_f = P_{H_2O} + P_{CO_2} = 450$ MPa, constructed using the Thermo-

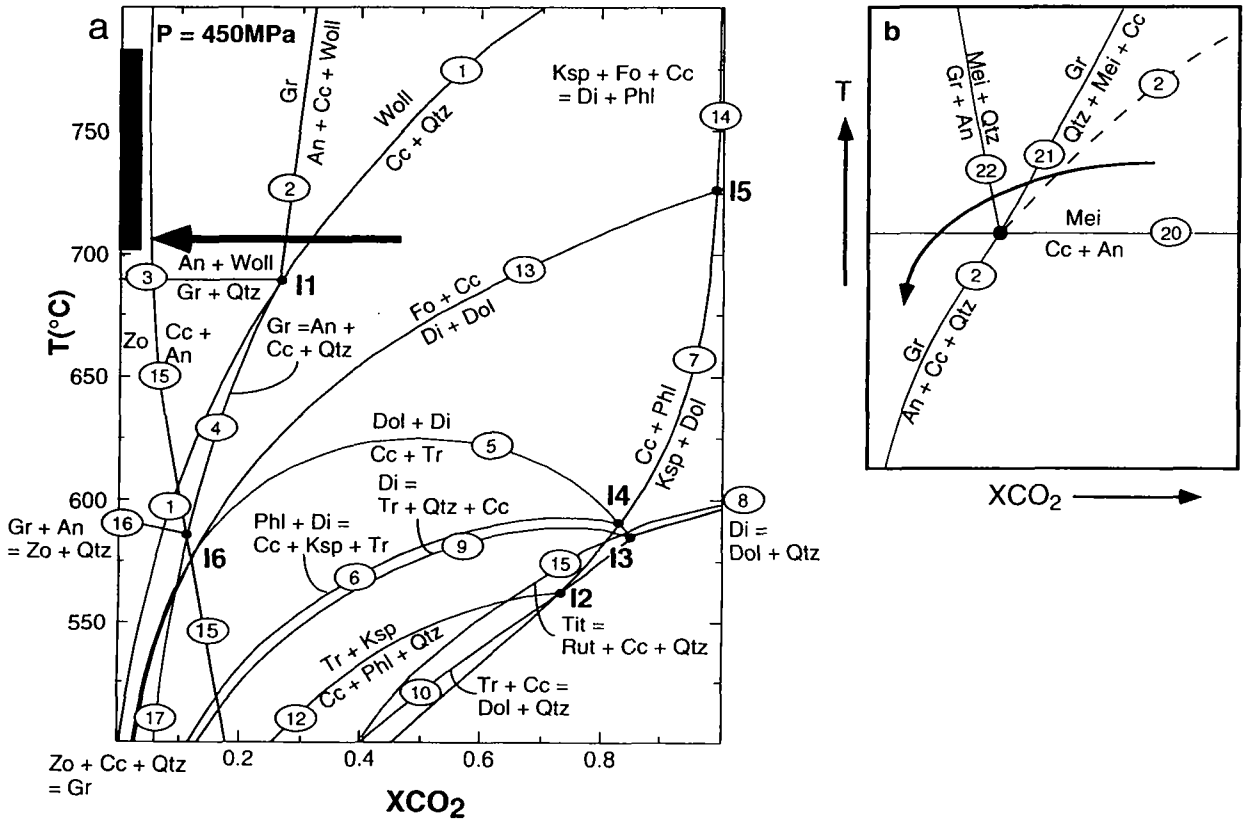

Fig. 4. (a) T–X_{CO_2} section in the system K_2O–CaO–MgO–Al_2O_3–SiO_2–H_2O–CO_2 (KCMAS) at $P_f = P_{H_2O} + P_{CO_2} = 450$ MPa, constructed using the Thermocalc computer program and the internally consistent thermodynamic dataset of Powell & Holland (1989) and Holland & Powell (1990) and showing selected reactions between anorthite, calcite, dolomite, diopside, forsterite, grossular, phlogopite, quartz, rutile, titanite, tremolite, zoisite, and an H_2O–CO_2 fluid. Solid area shows the peak metamorphic temperatures for the study area. Infiltration of water-rich ($X_{CO_2} = 0.1$–0.3) fluids depicted by the arrow occurred at close to peak-metamorphic temperatures. (b) Schematic T–X_{CO_2} section showing that the reaction and pseudomorph textures involving scapolite (Fig. 3b) may be explained by the infiltration of water-rich fluids during or followed by cooling. The grossular rims probably formed by reaction (21), with the later breakdown of scapolite to calcite and anorthite by reaction (20).

calc computer program and the internally consistent thermodynamic dataset of Powell & Holland (1989) and Holland & Powell (1990), and showing selected reactions between anorthite, calcite, diopside, dolomite, forsterite, grossular, phlogopite, quartz, rutile, titanite, tremolite, zoisite and an H_2O–CO_2 fluid. Because insufficient mineral composition data exist to draw quantitative pseudosections for calcsilicates, end-member mineral compositions were used in the construction of Fig. 4(a). The minerals in the rocks contain non-KCMAS components that increase the variance of the mineral assemblages; however, Fig. 4(a) provides a general framework in which to discuss fluid infiltration. The displaced positions of certain equilibria were calculated using the following mineral compositions based on the analyses in Table 2: grossular ($Gr_{0.80}$); phlogopite ($Phl_{0.40}$); forsterite ($Fo_{0.74}$); and diopside ($Di_{0.87}$). Following Harley & Buick (1992) and Buick *et al.* (1994b), activity–compositional relationships for grossular–andradite solid solutions were modelled using the asymmetric a–X models of Engi & Wersin (1987), with corrections as noted by Harley & Buick (1992) and the minor pyrope and spessartine components treated as ideal diluents. Diopside, forsterite, and phlogopite were treated as ideal solutions. The numerous reactions that involve other calcsilicate minerals such as akermanite, tilleyite, monticellite, rankinite, merwinite, spurrite, larnite and kilchoanite are not shown, as they occur at more water-rich conditions than reactions on Fig. 4(a) that limit the fluid compositions (e.g. Tracy & Frost, 1991).

Wollastonite marbles

Except in very high-temperature contact metamorphic environments (e.g. Valley *et al.*, 1990), the formation of wollastonite in marbles requires the infiltration of water-rich fluids (Cartwright & Valley, 1991; Ferry, 1991). Marbles that contain relatively low volumes of wollastonite with garnet occurring along calcite–plagioclase and calcite–quartz grain boundaries preserve evidence of the reaction

$$2Cc + An + Qtz = Gr + 2CO_2 \quad (4)$$

which in the end-member CAS system lies below I1. The minor andradite component of the garnet in these zones may be explained by the involvement of clinopyroxene via a reaction such as

$$4Cc + 4Qtz + 2Ess = Gr + Ad + 4CO_2$$

(Buick *et al.*, 1993). Much of the wollastonite was probably formed by the reaction

$$Cc + Qtz = Woll + CO_2. \quad (1)$$

Growth of grossular between wollastonite and calcite or wollastonite and plagioclase implies that the reaction

$$Cc + Woll + An = Gr + CO_2, \quad (2)$$

which lies at higher temperatures than I1, was crossed. The minor andradite component of this garnet may also be explained by involving clinopyroxene via a reaction such as

$$4Ess + 8Cc = 2Gr + 2Ad + 8CO_2.$$

The involvement of reactions lying both above and below I1 is best explained by slight changes in bulk composition, the more Fe-rich rocks intersecting reaction (4), whereas the more Mg-rich compositions intersect reaction (2) at the same P–T conditions. Using the measured mineral compositions suggests that the wollastonite marbles equilibrated at *c.* 700° C, implying that these rocks were infiltrated by water-rich fluids at slightly below peak metamorphic temperatures (*c.* 740° C). Since the wollastonite encloses, and hence is inferred to postdate, the $S2_2$ fabric that is elsewhere defined by the highest grade minerals, fluid flow is most likely to have occurred during the earliest stages of cooling. Because many samples in the wollastonite marbles do not contain quartz and none contains minerals such as zoisite (stable at lower X_{CO_2} values than reaction 15), fluid compositions are constrained to have been between $X_{CO_2} = 0.1$ and 0.3.

Oxygen fugacities for the grandite-rich zones and the marbles were estimated from the reaction

$$4Hed + 2Cc + O_2 = 2Ad + 2Qtz + 2CO_2,$$

again using Thermocalc (Powell & Holland, 1989) and the internally consistent thermodynamic dataset of Holland & Powell (1990). For the grandite-rich zones a garnet composition of $Ad_{0.54}$ and a clinopyroxene composition of $Hed_{0.18}$ were assumed, whereas for the marbles garnet and clinopyroxene compositions of $Ad_{0.20}$ and $Hed_{0.15}$ were used. Calcite and quartz were assumed to be pure. Hedenbergite activities were calculated assuming ideal mixing and andradite activities were calculated as outlined above. For an X_{CO_2} of 0.2, a pressure of 400 MPa and a temperature of 700° C, $\log fO_2$ values (expressed using a 1-bar standard state) are approximately −11 for the grandite-rich zones and −12 for the marbles. These values are maxima because quartz is generally not stable with the garnet-bearing assemblages. Varying the assumed X_{CO_2} between 0.1 and 0.3 results in a variation in $\log fO_2$ of ±0.25. Uncertainties in pressure of ±50 MPa and in temperature of ±20° C translate into uncertainties of ±0.1 and ±1 log unit, respectively. Overall, these fO_2 values are close to those of the haematite–magnetite buffer (log $fO_2 = -11.9$ at the conditions used above: Myers & Eugster, 1983; Powell & Holland, 1989). Similar oxidation states were calculated for contact metamorphic grandite-bearing skarn layers in marbles from the Lower Calcsilicate unit of the Reynolds Range Group (Buick *et al.*, 1993).

No direct measurement of scapolite compositions could be made; hence the use of scapolite to determine minimum pressures and temperatures of metamorphism (e.g. Harley & Buick, 1992) is not possible. From the textural data discussed above, the sequence of reactions for scapolite breakdown in the end member CAS system was probably

$$Mei + 5Cc + 3Qtz = 3Gr + CO_2 \quad (21)$$

followed by

$$Mei = Cc + 3An \quad (20)$$

(Fig. 4b). Given that mineral assemblages in the marble imply that reaction (2) has been crossed, these changes are broadly consistent with the infiltration of water-rich fluids during cooling. As for the reactions discussed above, the actual reactions probably involved clinopyroxene to form the andradite component of garnet.

Calcite and dolomite marbles

By contrast with the wollastonite marbles, the assemblages in the wollastonite-free calcite or dolomite marbles could be formed by internal buffering with no or negligible fluids. The assemblage calcite + quartz + diopside + K-feldspar ±titanite that is commonly found in the calcite marbles is stable at peak metamorphic conditions at X_{CO_2} values of ≥0.3. The phlogopite that is present in a few calcite marbles is not predicted to be stable at peak metamorphic conditions, as reaction (12) is the upper limit of phlogopite stability in calcite + quartz assemblages. Using actual mineral compositions this phlogopite is predicted to break down to diopside + K-feldspar at *c.* 630° C. The phlogopite possibly persisted metastably due to being surrounded by calcite. Overall, there is little petrological evidence for fluid infiltration in the calcite marbles; however, resetting of the oxygen-isotope ratios at the margin of the wollastonite marbles (discussed below) suggests at least local fluid infiltration. The dolomite marble contains the assemblage forsterite + diopside + K-feldspar + phlogopite + calcite + dolomite, which is stable at I5 in the end-member KCMAS system. Using the measured mineral compositions this assemblage constrains temperatures to be *c.* 700° C, broadly consistent with peak metamorphic temperatures in this area, with an X_{CO_2} close to 1. Such high X_{CO_2} assemblages are predicted to form in dolomite marbles that have not been infiltrated by significant volumes of water-rich fluids where mineral assemblages are formed dominantly by internal buffering (Ferry, 1991).

Marl layers

The marl layers both within and outside the wollastonite marbles contain similar assemblages. Significantly, marls within the wollastonite marbles contain calcite and quartz with no wollastonite. These data suggest that, even though the wollastonite marbles record significant fluid infiltration, the interlayered marls were not infiltrated by large volumes of fluid during metamorphism. As discussed below, the stable isotope data are also consistent with this conclusion. Some marl layers in the calcite marbles contain dolomite + K-feldspar that in KCMAS lies at very high X_{CO_2} (on or above reaction 7), and again the evolution of these rocks was probably dominated by internal buffering.

STABLE ISOTOPE DATA

Stable isotope geochemistry of calcareous rocks has successfully been used in many terranes to study fluid–rock interaction (e.g. Ganor *et al.*, 1989; Bickle & Baker, 1990; Cartwright & Valley, 1991; Ferry & Dipple, 1992; Nabelek *et al.*, 1992; Bowman & Willet, 1992; Todd & Evans, 1993; Cartwright & Weaver, 1993; Cartwright, 1994; Cartwright & Oliver, 1994). In this study, samples were collected from a composite traverse running across strike and from other localities in the high-grade region of the Reynolds Range (Tables 3a,b and Fig. 2). The results will be discussed for individual rock types. To investigate small-scale isotopic heterogeneities, multiple analyses were made on several hand samples. Samples designated A, B in Tables 3a and b represent multiple centimetre-thick slabs from a single hand specimen. Weight percent calcite data in Table 3 were estimated from calcite dissolution. The calcite contents of the wollastonite marbles vary between those of the 'wollastonite-rich' and 'wollastonite-poor' zones in Table 1, suggesting that some integration of these zones may have occurred during sampling. Possible consequences of mechanical integration during sampling on the interpretation of the stable isotope data are discussed below.

Table 3a. Stable isotope ratios of calcite and dolomite marbles.

Sample*	Distance (m)†	No. of samples‡	%Cc	$\delta^{13}C$ Cc	$\delta^{18}O$ Cc	Di	Δ(Cc–Di)
136A Mbl¶	20.8	1	61	−0.6	14.6		
136B Mbl¶	20.8	2	65–71	−0.7 to −0.5	17.7–15.5		
137 Mbl	22.5	1	66	−0.6	14.1	12.3	1.8
138 Mbl	40.5	2	77–84	−0.4 to −0.4	16.3–16.5		
138 Marl	40.5	1	5	−0.4	17.4		
139 Mbl	44.1	1	75	0.0	16.5		
140 Marl	45.3	1	9	−0.5	17.7		
140 Mbl	45.3	1	85	−0.3	18.7	16.6	2.1
141A Mbl	45.4	1	73	−0.3	18.6	16.8	1.8
141B Marl	45.4	4	5–8	−0.4 to −0.2	17.2–18.7		
141B Mbl	45.4	3	78–88	−0.6 to −0.4	18.4–18.6		
142 Mbl	46.9	1	90	−0.3	17.4		
143A Marl	47.7	1	7	−0.6	18.1		
143A Mbl	47.7	1	78	−0.3	17.6	16.1	1.5
143B Marl	47.7	3	8–15	0.1 to 0.2	17.8–18.3		
143B Mbl	47.7	3	81–82	−0.7 to 0.6	17.6–17.8		
146 Mbl§	48.6	1	72	−0.3	16.7		
147A Marl	50.9	1	3	0.7	18.9		
147A Mbl	50.9	1	70	−0.3	17.8	15.6	2.2
147B Marl	50.9	2	7–8	0.0 to 0.1	18.2–18.6		
147B Mbl1	50.9	4	63–72	−0.6 to–0.4	17.5–17.8		

*Samples = 9235 unless otherwise noted. †Distance from boundary between wollastonite marble and calcite marble. ‡Number of multiple drilled samples from individual slabs. §Dolomite marble. ¶A, B = slabs from same sample.

Table 3b. Stable isotope ratios of wollastonite marbles.

Sample*	Distance (m)†	No. of samples‡	%Cc	$\delta^{13}C$ Cc	$\delta^{18}O$ Cc	Woll	Δ(Cc–Woll)
119 Marl	2	1	11	−2.4	15.6		
119 Mbl	2	1	28	−2.1	15.6		
120 Mbl	2.4	1	10	−3.0	13.9		
121A Marl	3	1	6	−0.7	15.3		
121A Mbl	3	1	14	−2.0	17.0	14.1	2.9
121B Mbl	3	2	9–15	−3.4 to −2.3	14.7–15.4		
122 Mbl	3.2	1	48	−1.3	16.7		
123A GZ	3.6	2	2–3	−5.9 to −5.0	11.3–11.5		
123A Marl	3.6	1	6	−1.1	14.9		
123A Mbl	3.6	1	7	−3.2	15.0	12.2	2.8
123B GZ	3.6	2	4–7	−7.1 to −4.0	9.8–11.2		
123B Marl	3.6	2	10–11	−2.2 to −1.9	15.3–17.4		
123B Mbl	3.6	8	4–14	−3.5 to −1.1	11.4–15.9		
124 Marl	5.2	1	5	−1.6	16.1		
125A Mbl	5.9	4	5–7	−1.0 to −0.2	15.4–16.4		
125A Marl	5.9	1	8	−1.0	17.4		
125B Mbl	5.9	1	6	−0.9	16.4	13.2	3.2
126 Mbl	7.5	1	61	−1.5	16.0		
127 Marl	8.8	1	7	0.7	15.1		
127 Mbl	8.8	1	31	−1.9	15.6		
129 GZ	10.3	1	5	−5.1	11.4		
129A Mbl	10.3	1	10	−0.7	17.3		
129B Mbl	10.3	1	46	−1.8	15.4	13.1	2.3
128 Mbl	10.3	1	47	0.1	17.6		
130 Mbl	13.8	1	23	−1.5	15.8	12.1	3.7
131 Mbl	15.4	1	51	−1.4	15.9	12.6	3.3
362 GZ	20.5	1	9	−3.4	14.2		
362 Marl	20.5	1	8	0.2	15.9		
362 Mbl	20.5	1	5	−2.9	13.8	12.9	0.9
363A Mbl	20.7	1	17	−1.5	15.0	12.2	2.8
363B GZ	20.7	1	5	−4.5	11.6		
363B Marl	20.7	3	14–20	−2.3 to −0.8	15.6–16.5		
363B Mbl	20.7	8	11–80	−3.0 to −0.3	12.1–18.5		
363B Vein	20.7	1		−0.8	14.2		
365 Mbl	21.5	3	7–43	−1.4 to −0.4	15.6–17.3		
366A Mbl	22.7	2	8–9	−1.9 to −1.4	16.4–16.7		
366A Marl	22.7	1	12	−0.6	16.4		
366B Marl	22.7	3	6–10	−0.6 to 0.6	16.4–18.2		
366B Mbl	22.7	8	4–15	−1.8 to 0.4	13.5–18.6		
368 Mbl	24.5	1	6	−0.9	15.9		
368A Mbl	24.5	1	17	−0.8	16.4		
368B Marl	24.5	2	8–9	−0.4 to −0.2	18.2–18.6		
368B Mbl	24.5	3	9–12	−3.1 to 0.2	13.4–18.2		
369 Mbl	24.7	1	26	−0.7	16.0	13.2	2.8
370 Mbl	24.8	1	52	−1.2	16.2		
9135-289 Mbl	Other¶	1	13	−2.5	14.5		
9135-290 Mbl	Other	1	8	−5.3	12.8		
9135-227 Mbl	Other	1	17	0.2	12.9		
9135-229 Mbl	Other	1	48	−0.9	17.4		
9135-262 Mbl	Other	1	14	−2.1	14.9		
9135-264 Mbl	Other	1	31	−0.1	16.1		

*Samples = 9235 unless otherwise noted. †Distance from boundary between wollastonite marble and calcite marble. ‡Number of multiple drilled samples from individual slabs. ¶Samples from wollastonite marbles elsewhere in the Upper Calcsilicate.

Calcite marbles

The stable isotope data for these rock types are shown in Table 3a and Figs 5–7. The following features are apparent: (1) the majority of $\delta^{18}O$(Cc) values are in the range 16–19‰ (average 17.2 ± 1.2‰), which are closely similar to $\delta^{18}O$ values of Upper Calcsilicate marbles in the high-grade Reynolds Range as a whole (*c.* 17.3 ± 1.2‰, $n = 47$; Buick & Cartwright unpubl. data); (2) two calcite marble samples that occur approximately 20 m from the margin of the wollastonite marbles have significantly lower $\delta^{18}O$(Cc) values (as low as 14.1‰); (3) local variations in $\delta^{18}O$ or $\delta^{13}C$ values are usually within ±0.5‰, except for one of the samples closest to the wollastonite marble (9235-136) where $\delta^{18}O$(Cc) values range from 14.6 to 17.7‰; (4) $\delta^{13}C$ values for the calcite marbles are *c.* −0.1 ± 0.4‰; and (5) the marls have similar $\delta^{18}O$(Cc) and $\delta^{13}C$(Cc) values to the marbles, despite having much lower calcite contents (<20 wt%).

Values of $\delta^{18}O$(Di) range between 12 and 17‰ (Table 3b, Fig. 7), and $\Delta^{18}O$(Cc–Di) values are *c.* 2‰, regardless of the $\delta^{18}O$(Cc) value of the rock. The ^{18}O fractionations are close to those expected at peak metamorphic temperatures, suggesting that the minerals in the calcite marbles approached isotopic equilibrium during the $M2_2$ event and did not undergo later, low-temperature, resetting.

Wollastonite marbles

The stable isotope data from the wollastonite marbles are shown in Table 3b and Figs 5–8. $\delta^{18}O$(Cc) values for these rocks vary from 18.6 to 11.4‰ with an average of 15.4 ± 1.6‰. These $\delta^{18}O$ values are much lower than the average $\delta^{18}O$(Cc) value of the calcite marbles (17.2 ± 1.2‰). $\delta^{13}C$(Cc) values for the wollastonite marbles vary from 0.4‰ to as low as −5.3‰, again much lower than $\delta^{13}C$(Cc) of the calcite marbles (−0.1 ± 0.4‰). The data show the following features, which must be explained by any models of fluid infiltration: (1) with the exception of a

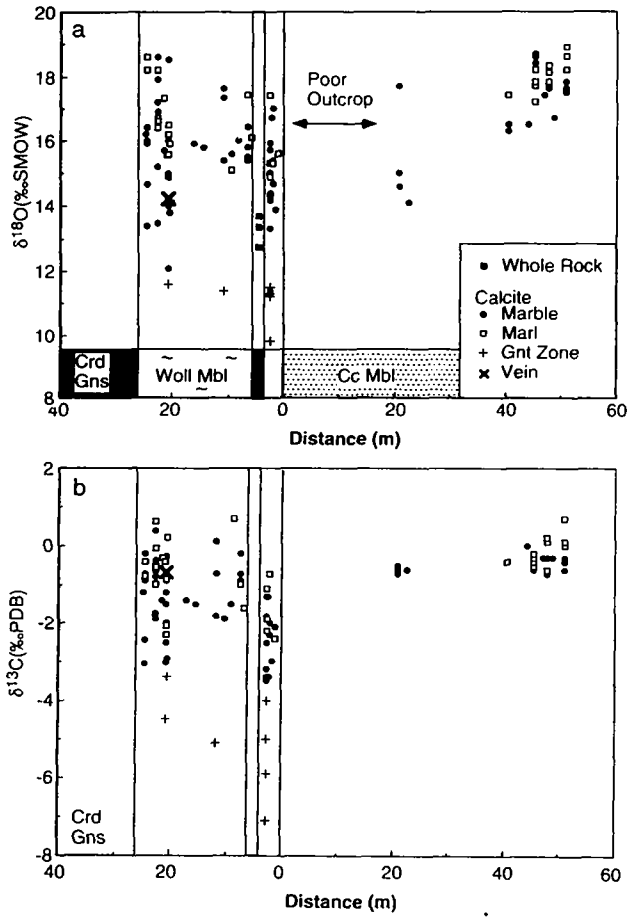

Fig. 5. Stable isotope ratios of Upper Calcsilicate rocks collected along the profile shown in Fig. 2 (data from Tables 3a and b). The calcite marbles show slightly lower $\delta^{18}O(Cc)$ values near to the contact with the wollastonite marbles. The $\delta^{18}O(Cc)$ (a) and $\delta^{13}C(Cc)$ (b) values of both marl and marble layers are in general lower and more variable in the wollastonite marbles than in the calcite marbles. Calcite from the grandite-rich zones (Gnt zone) have lower $\delta^{18}O(Cc)$ and $\delta^{13}C(Cc)$ values than that of the marls and the marbles. The lowering of $\delta^{18}O(Cc)$ and $\delta^{13}C(Cc)$ values in the wollastonite-bearing rocks is probably due to fluid infiltration, and the highly variable isotopic ratios suggest that the volumes of infiltrating fluid varied significantly on a small scale.

few samples, the wollastonite marbles have lower $\delta^{13}C(Cc)$ and wt% calcite values than the calcite marbles; (2) $\delta^{18}O(Cc)$ and $\delta^{13}C(Cc)$ values define a moderate linear trend ($r^2 \approx 0.7$); (3) the grandite-rich zones lie at the lower end of the $\delta^{18}O(Cc)$ vs. $\delta^{13}C(Cc)$ trend, and have low wt% calcite contents; (4) $\delta^{18}O(Cc)$ values of different samples from each rock may vary by several permil; (5) the $\delta^{18}O(Cc)$ and $\delta^{13}C(Cc)$ values of the marls within the wollastonite marbles are slightly lower and more variable (16.4 ± 1.1‰ and -0.9 ± 0.9‰, respectively) than those of the marls in the calcite marbles (18.0 ± 0.5‰ and -0.1 ± 0.4‰, respectively); and (6) for the samples collected from the traverse across the single wollastonite layer, there is little correlation between $\delta^{18}O$ and the distance from the calcite marble or from the cordierite-gneiss layers.

In the wollastonite marbles, $\delta^{18}O(Woll)$ values range between 12 and 14‰ (Table 3b; Fig. 7). Although there is a general correlation between $\delta^{18}O(Woll)$ and $\delta^{18}O(Cc)$, it is not as regular as the correlation between $\delta^{18}O(Cc)$ and $\delta^{18}O(Di)$ in the calcite marbles. $\Delta^{18}O(Cc\text{–}Woll)$ values vary from 1 to 3‰, corresponding to apparent isotopic temperatures of 400 to ≥700° C. The variation in $\Delta^{18}O(Cc\text{–}Woll)$ may reflect isotopic disequilibrium due to differential resetting at low temperatures after the peak of $M2_2$ metamorphism. However, given the large heterogeneity in $\delta^{18}O(Cc)$ values in individual samples (Table 3b), it is likely that the variation in $\Delta^{18}O(Cc\text{–}Woll)$ values results, at least in part, from the sampling process. Since wollastonite mineral samples were separated from *c.* 1 cm^3 cubes, whereas the calcite samples were drilled from smaller areas, mechanical integration of wollastonite from multiple zones that have calcite (and possibly wollastonite) with different $\delta^{18}O$ values (Fig. 7) is probably unavoidable. As there is no mineralogical evidence of later lower-temperature fluid flow in these rocks, we consider that the scatter in $\Delta^{18}O(Cc\text{–}Woll)$ values is largely the result of integration during the sample preparation.

Small-scale isotopic heterogeneity

Critical to any discussion of fluid infiltration is the scale and degree of isotopic heterogeneity. Uniform $\delta^{18}O$ and $\delta^{13}C$ values on the scale of a few centimetres to a few metres are most consistent with the rocks equilibrating with a pervasive fluid on that scale; however, centimetre-scale isotopic heterogeneities may be most consistent with channelled fluids (e.g. Cartwright & Weaver, 1993; Cartwright, 1994; Cartwright & Oliver, 1994) or with later resetting of isotopic ratios, for instance by metamorphic reactions (e.g. Buick *et al.*, 1994b). Figure 9 shows the distribution of stable isotope ratios in three samples of wollastonite marble. As is evident from Figs 5 and 6, a range of both $\delta^{13}C(Cc)$ and $\delta^{18}O(Cc)$ values close to the total range of isotopic ratios in this group of samples as a whole occurs within individual samples. The spatial pattern of isotopic resetting is in general irregular (probably reflecting the intensely variable fluid fluxes, as inferred from the petrological data); however, some trends do exist. For example, in 9235-368 the $\delta^{13}C(Cc)$ and $\delta^{18}O(Cc)$ values of the marble approach those of the marl toward the contact with the marl (there is no grandite-rich zone at this contact). As discussed below, this type of trend argues for some fluid–rock interaction between the marbles and the marls in the wollastonite rocks. In 9235-361, an area of uniform marble $\delta^{13}C(Cc)$ and $\delta^{18}O(Cc)$ values −0.9‰ and 14.9‰ may represent a zone that has undergone a relatively uniform degree of fluid–rock interaction. In general, the marl layers have higher $\delta^{18}O(Cc)$ and $\delta^{13}C(Cc)$ values and the grandite-rich zones have lower $\delta^{18}O(Cc)$ and $\delta^{13}C(Cc)$ values than the surrounding marbles; steep gradients in $\delta^{13}C(Cc)$ and $\delta^{18}O(Cc)$ values of up to 4–5‰ in 1–2 mm are preserved at their margins. Hence, in contrast to the general situation where high-temperature metamorphic fluid flow homogenizes

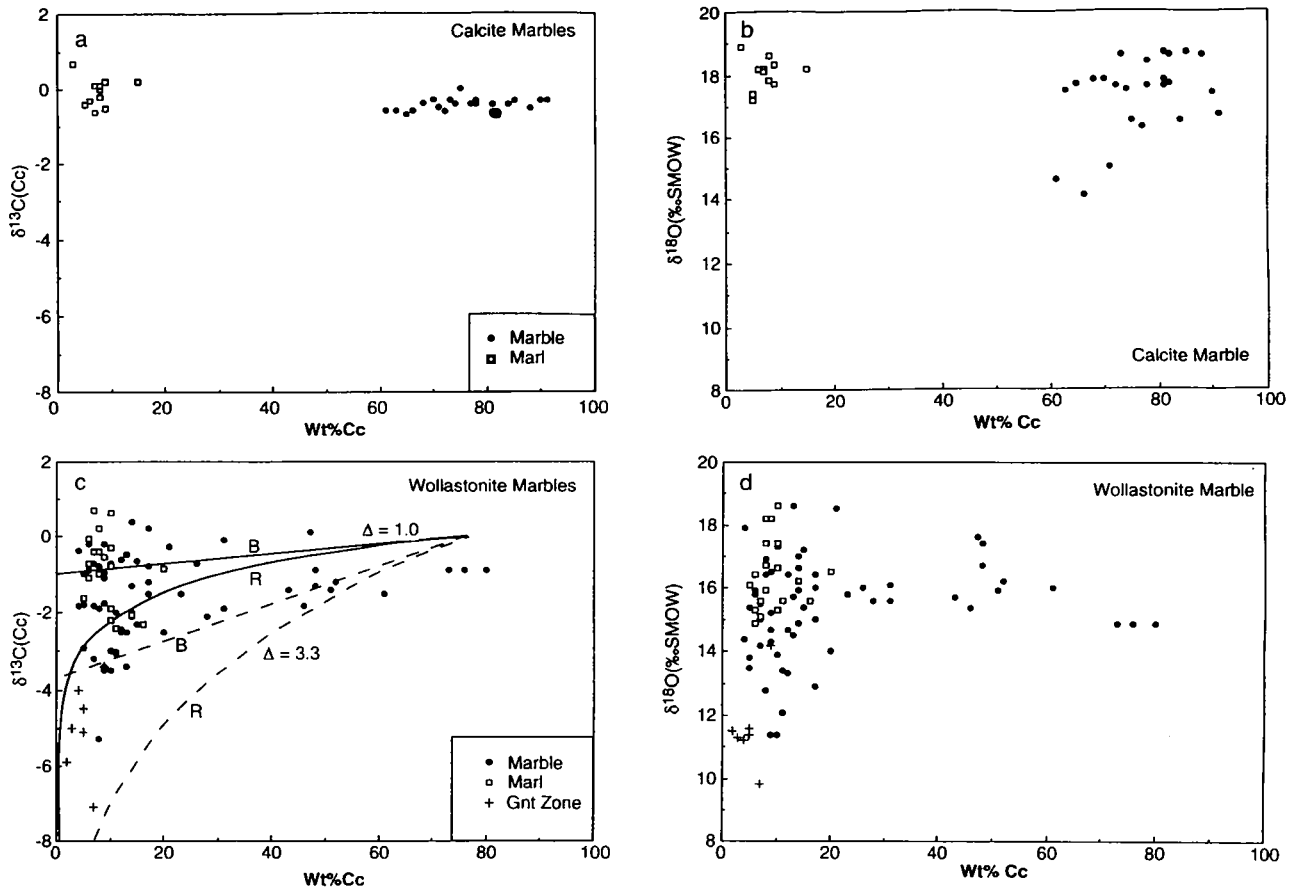

Fig. 6. Stable isotope ratios of calcite vs. the calcite contents of the Upper Calcsilicate rocks (data from Tables 3a and b). There is little correlation between $\delta^{13}C(Cc)$ (a) or $\delta^{18}O(Cc)$ (b) and calcite content in the calcite marbles. The marl layers have similar $\delta^{18}O(Cc)$ and $\delta^{13}C(Cc)$ values to the marbles despite their much lower calcite contents. The wollastonite marbles have much lower $\delta^{18}O(Cc)$ (d) and $\delta^{13}C(Cc)$ (c) values, especially at low calcite contents. However, the shift in $\delta^{13}C(Cc)$ values is much less than that predicted by devolatilization using calcite-CO_2 ^{13}C fractionations (c, dashed lines) while a much lower ^{13}C fractionation ($\Delta^{13}C \approx 1$) fits the data better (solid lines). This apparent discrepancy may reflect the speciation of C in water-rich metamorphic fluids.

stable isotope gradients, fluid flow in the Upper Calcsilicate produced very heterogeneous $\delta^{18}O$ and $\delta^{13}C$ values in rocks that initially were characterized by only small variations in isotopic ratios.

Pegmatites and cordierite gneisses

The aluminous pegmatites within the Upper Calcsilicate Unit have $\delta^{18}O$ values of 10.1–12.1‰ (average = 10.9 ± 0.7‰; Table 4; Fig. 10). Minerals from within the pegmatites have concordant, high-temperature, oxygen isotope fractionations [$\delta^{18}O(Qtz) = 11.3–13.5‰$; $\delta^{18}O(Plg) = 10.0–11.2‰$; $\delta^{18}O(Crd) = 9.4‰$; $\delta^{18}O(Sill) = 10.2–10.3‰$; $\delta^{18}O(Bt) = 8.1–8.9‰$]. The $\delta^{18}O$ values of the aluminous pegmatites are in the range of $\delta^{18}O$ values recorded from metapelites in the high-grade parts of the Reynolds Range (6–15‰: Buick & Cartwright, unpubl. data). The thin cordierite gneisses that occur adjacent to and within the wollastonite marble layer have $\delta^{18}O$ values of 12.4–13.7‰ (Table 4; Fig. 10).

DISCUSSION

The rocks in the Upper Calcsilicate Unit of the Reynolds Range underwent heterogeneous fluid infiltration during $M2_2$. The petrology and stable isotope geochemistry of these rocks may be used to evaluate the patterns and processes of fluid infiltration.

Silica metasomatism: formation of excess wollastonite

Some wollastonite in the marbles was almost certainly formed by reaction (1). However, the calcite marbles contain 6–11% quartz (2600–4800 mol/m^3), and even if all quartz was consumed in the formation of wollastonite, the wollastonite marbles should contain <19% wollastonite. This is a maximum value, as some quartz would have been used to form grossular by reaction (4). Unless the marbles that contain high volumes of wollastonite had much higher initial quartz contents (*c.* 38%) which, given the relative

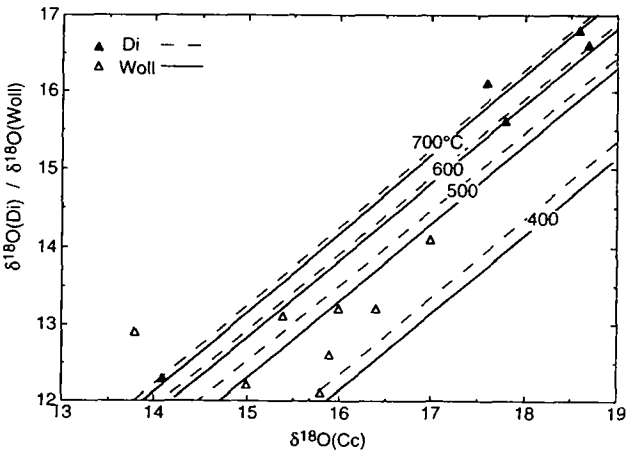

Fig. 7. Summary of ^{18}O fractionations between calcite and diopside from the calcite marbles and calcite and wollastonite from the wollastonite marbles (data from Tables 3a and b, fractionations from Matthews *et al.*, 1983; Clayton *et al.*, 1989). Minerals in the calcite marbles preserve close to peak-metamorphic isotopic fractionations. By contrast minerals in the wollastonite marbles show a much higher degree of scatter, which is probably due to small-scale heterogeneities in calcite (and possibly wollastonite) $\delta^{18}O$ values.

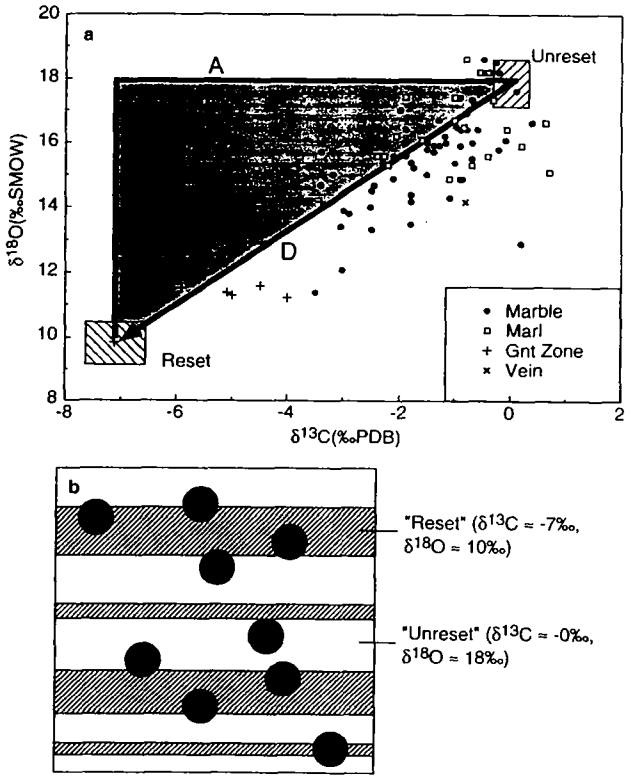

Fig. 8. (a) $\delta^{18}O(Cc)$ vs. $\delta^{13}C(Cc)$ values from the wollastonite-bearing rocks. There is a strong correlation between the $\delta^{18}O(Cc)$ and $\delta^{13}C(Cc)$ values of the marbles and the grandite-rich zones that extends to lower $\delta^{18}O$ and $\delta^{13}C$ values than those of the calcite marbles (Unreset box). However, this trend is dissimilar to ones that are predicted to form due to the infiltration of water-rich fluids where advection dominates (line A). Rather, the trend is similar to that predicted due to dispersion (line D). If fluids were perfectly channelled (b) the sampling procedures used could have mechanically integrated reset and unreset zones to produce the trend (filled circles); however, such perfect channelling is unlikely. Transverse dispersion could explain the observed trend again only if channelling formed a bimodal set of reset and unreset zones. It is considered most likely that the observed $\delta^{18}O(Cc)$ vs. $\delta^{13}C(Cc)$ trend reflects combined fluid infiltration and devolatilization.

mineralogical homogeneity of the calcite marbles in the Upper Calcsilicate seems unlikely, the formation of large volumes of wollastonite must reflect other reactions. There is little difference in K-feldspar or diopside contents between the wollastonite marbles (1–7% and 5–13%, respectively) and their unmetasomatized equivalents (0–6% and 5–14%, respectively), suggesting that the excess wollastonite does not result from the loss of components (e.g. Ca). Rather, we suggest that the wollastonite is the product of silica metasomatism by a reaction such as

$$Cc + SiO_{2(aq)} = Woll + CO_2, \qquad (1A)$$

which causes relatively little volume change (calcite has a molar volume of 36.9 cm^3 and wollastonite of 39.9 cm^3; Robie *et al.*, 1978). Reaction (1A) has been proposed to account for metasomatism of calcsilicates in other terranes (e.g. Barton *et al.*, 1991; Gerdes & Valley, 1994). As discussed below, variations in the modal proportion of wollastonite help constrain the direction of fluid flow and relative fluid fluxes.

Silica metasomatism may be a common feature of metamorphosed marbles. Figure 11 shows the estimated solubility of silica in fluids in equilibrium with calcite + quartz and calcite + wollastonite assemblages at 400 MPa. At or below reaction (1) quartz is stable; hence the activity of quartz = 1. At higher temperatures or lower X_{CO_2} values than those of reaction (1), the activity of quartz decreases progressively. Since the equilibrium concentration of $SiO_{2(aq)}$ in the fluid is proportional to the activity of quartz, this too decreases as X_{CO_2} decreases. Consider a marble that contains calcite with a small volume of quartz at *c.* 650° C. The infiltration of a water-rich fluid ($X_{CO_2} = 0.1$) will cause reaction (1) to occur, removing the quartz and forming calcite + wollastonite. If this fluid was initially in equilibrium with silica-saturated rocks, it would have contained 15–20 g/kg $SiO_{2(aq)}$. However, fluids in equilibrium with calcite + wollastonite at 400 MPa, 650° C, and $X_{CO_2} = 0.1$ only contain *c.* 12 g/kg $SiO_{2(aq)}$; hence fluid infiltration will also cause silica to precipitate. If calcite is present, this silica will form wollastonite via reaction (1A). Although Fig. 11 is a simplification (especially as it neglects the effects of variable CO_2:H_2O ratios on silica solubility), it does illustrate that the infiltration of water-rich fluids from silica-saturated rocks into marbles will probably result in the formation of some wollastonite, due to the change in the equilibrium $SiO_{2(aq)}$ contents of the fluid.

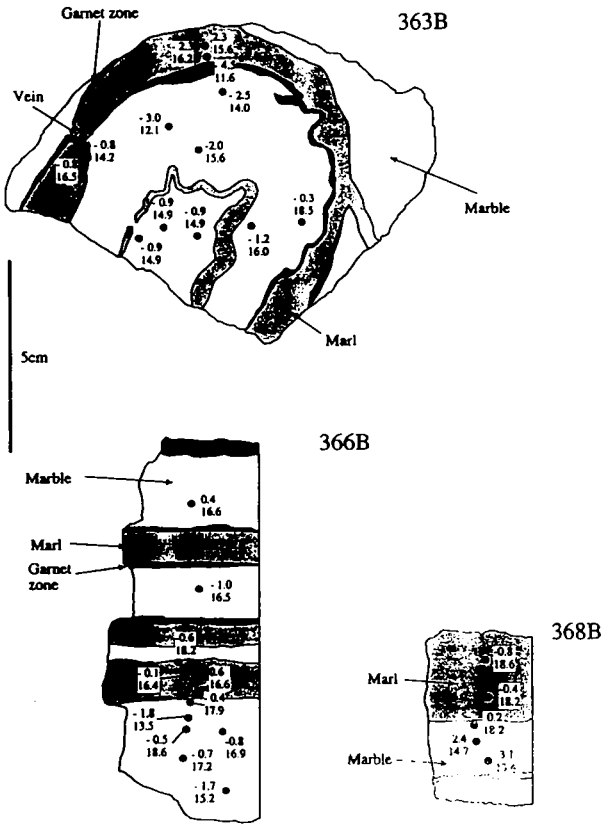

Fig. 9. The distribution of stable isotope ratios in the wollastonite-bearing rocks (data from Table 3b). The great range in both $\delta^{13}C(Cc)$ and $\delta^{18}O(Cc)$ values within individual samples is similar to the total range of isotopic ratios (Fig. 6). The spatial pattern of isotopic resetting is irregular, probably reflecting the intensely variable fluid fluxes as inferred from the petrological data; however, some trends exist. In 9235-368B the $\delta^{13}C(Cc)$ and $\delta^{18}O(Cc)$ values of the marble approach those of the marl which suggests some fluid–rock interaction between the marble and the marl. In 361, an area of uniform marble $\delta^{13}C(Cc)$ and $\delta^{18}O(Cc)$ values may represent a zone of relatively uniform fluid–rock interaction. In general, the marl layers have higher $\delta^{18}O(Cc)$ and $\delta^{13}C(Cc)$ values and the grandite-rich zones have lower $\delta^{18}O(Cc)$ and $\delta^{13}C(Cc)$ values than the surrounding marbles, and steep gradients in $\delta^{13}C(Cc)$ and $\delta^{18}O(Cc)$ values of up to 4–5‰ in 1–2 mm are preserved.

Table 4. Stable isotope geochemistry of cordierite gneisses and aluminous pegmatites.

	$\delta^{18}O$ (‰)				
Sample	WR	Crd	Qtz	Sill	Bt
Cordierite gneisses					
9235-132	13.4				
9235-133	13.7				
9235-153	12.9				
Aluminous pegmatites					
R493-48	11.8		13.5		
R493-120	11.3				
R493-122	10.5	9.4	11.9		
R493-122	10.5	9.4	11.9		
R493-123	12.1				
R493-124	10.6		11.6	10.3	8.1
R493-127	10.1		11.4		8.4
R493-133	10.1		11.3		8.9
R493-135	10.5		11.3	10.3	

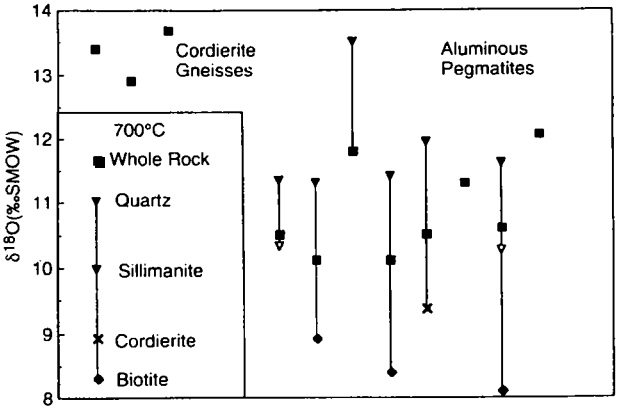

Fig. 10. Whole-rock and mineral $\delta^{18}O$ values of silicate rocks. The cordierite gneisses have $\delta^{18}O$ values of 13–14‰, which are probably too high for them to be the source of the fluids that infiltrated the marbles. The aluminous pegmatites that were emplaced soon after the peak of $M2_2$ metamorphism have appropriate $\delta^{18}O$ values (WR = 10–12‰) and ages to be the source of the fluids. Inset: the approximate ^{18}O fractionations at 700° C (data from Friedman & O'Neil, 1977; Clayton *et al.*, 1989; and calculated using the data of Zheng, 1993).

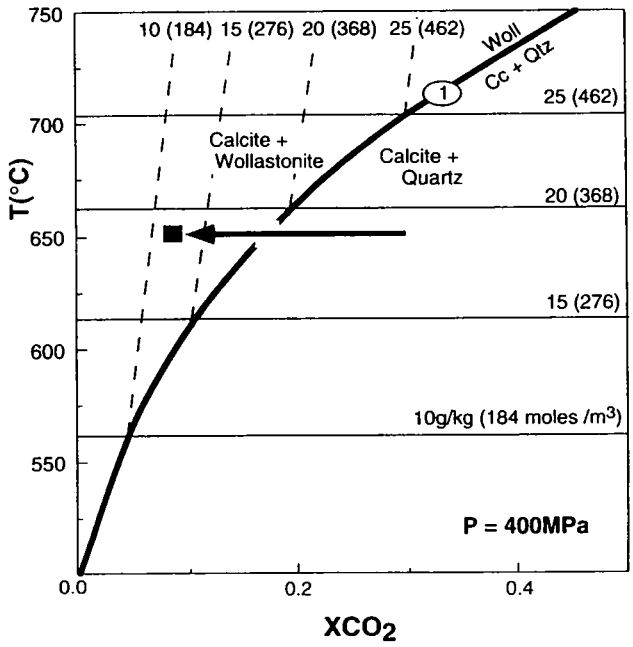

Fig. 11. Estimated concentrations of aqueous silica in fluids in equilibrium with quartz-bearing (solid lines) and calcite + wollastonite-bearing (dashed lines) assemblages (data derived from Barton *et al.*, 1991, their fig. 8). Concentrations are labelled in g/kg and mol/m^3 (converted using the data of Robie *et al.*, 1978). In the calcite + wollastonite field, the equilibrium concentrations of $SiO_{2(aq)}$ in quartz-bearing assemblages are much higher than in calcite + quartz-bearing assemblages; hence, fluid infiltration from a quartz-bearing rock may cause wollastonite formation by silica metasomatism via reaction (1A). Filled box and arrow illustrate fluid flow discussed in text.

Direction of fluid flow and variations in time-integrated fluid fluxes

The resetting of stable isotope ratios in the calcite marbles closest to the wollastonite marbles (Fig. 5) possibly reflects fluid flow from the silicate rocks across the wollastonite marbles into this unit. As has been outlined in a number of studies (e.g. Bickle & McKenzie, 1987; Baumgartner & Rumble, 1988; Cartwright & Valley, 1991) decoupling of hydration and isotopic fronts can occur during fluid advection or diffusion. The change in concentration of a chemical component (C_i) with time (t) during fluid infiltration is described by

$$\phi\left(\frac{\partial C_i}{\partial t}\right) = -\nabla.(C_i \bar{V} v_m) + D_e \nabla^2(C_i) + R_i \qquad \text{(i)}$$

where t is time, ϕ is porosity, v_m is the molar Darcy fluid flux, D_e is the combined effective diffusion–dispersion coefficient, $\bar{V}$ is the molar volume of the fluid, and R_i is the rate of production or consumption of component i during reaction (e.g. Bear, 1972; deMarsily, 1985). During metamorphic events, diffusive mass transport probably only occurs over a few centimetres to a few metres (e.g. Ganor *et al.*, 1989; Cartwright & Valley, 1991; Todd & Evans, 1993; Cartwright, 1994) and metamorphic reactions at high temperature do not generally produce significant changes in oxygen isotope ratios (e.g. Chamberlain *et al.*, 1990). Hence, in common with many studies, we will initially only consider isotopic resetting due to fluid advection, as this is usually the most important process.

For the transport of oxygen isotopes, the above simplifications reduce equation (i) to

$$q_m = \frac{z_a V_r}{N_f} \qquad \text{(ii)}$$

(Bickle & Baker, 1990; Dipple & Ferry, 1992) where q_m is the time-integrated molar fluid flux (mol/m^2), N_f is the number of moles of O per mole of fluid ($N_f = 1$ for H_2O and 2 for CO_2), and V_r is the number of moles of oxygen per m^3 of rock (*c.* 8.1×10^4 mol/m^3; e.g. Robie *et al.*, 1978). For resetting of mineral assemblages, if the infiltrating fluid is H_2O, Baumgartner & Ferry (1991) showed that equation (i) reduces to

$$q_m = \xi_{max}\left(\frac{v_i z_a}{X_i} - \Sigma v_j z_a\right) \qquad \text{(iii)}$$

where v_i is the stoichiometric coefficient of species i (in this case CO_2) in a reaction, Σv_j is the sum of the stoichiometric coefficients of all the fluid species in the reaction, X_i is the X_{CO_2} at which the reaction occurs, and ξ_{max} is the reaction progress required for the reaction to go to completion. The reaction calcite + quartz = wollastonite + CO_2 occurs at $X_{CO_2} \approx 0.3$ at the conditions of metamorphism. Assuming that the average marble had *c.* 8% (3500 mol/m^3) quartz prior to fluid infiltration yields $\xi_{max} = 3500$ mol/m^3. The width of the wollastonite marble is 40–45 m; if this is taken as the value of za, $q_m = c.\ 3.5 \times 10^5$ mol/m^3. Substituting these fluid fluxes into equation (ii) yields a distance of *c.* 8–9 m over which resetting of oxygen isotopes should have occurred. Thus, these calculations predict that the isotopic front should be behind the mineralogical front.

As noted above, there is too much wollastonite in the wollastonite marbles to be explained simply by the progress of reaction (1). The width of the zone of silica metasomatism may also be addressed using equation (ii). At 650° C and 400 MPa, the aqueous silica content of water-rich fluids in equilibrium with a silica-saturated rock is *c.* 16–17 g/kg, or *c.* 300 mol/m^3 (Barton *et al.*, 1991; Fig. 11). Where unmetasomatized, the marbles contain approximately 20 wt% SiO_2. These values yield $N_f \approx 5.4 \times 10^{-3}$ moles SiO_2 per mole of fluid and $V_r \approx 8.8 \times 10^3$ moles SiO_2 per m^3 rock. Substituting these values into equation (ii) and the value of $q_m = 3.5 \times 105$ mol/m2 calculated above yields $z \approx 0.2$ m. The results of this calculation are not significantly changed by moderate variations in the SiO_2 content of the rock and, since a silica-saturated fluid has been assumed, the distance calculated is a maximum.

Despite the fact that the partition coefficients for metasomatic reactions are poorly known and the amount of silica in the rock changes with metasomatism, the above approach can be used to make general comments on across-strike fluid flow. If across-strike fluid flow had occurred, the modal percentage of wollastonite should decrease markedly a few metres into the wollastonite marble as the limit of metasomatic alteration by reaction (1A) is reached. There then should be a zone of marbles with wollastonite contents that could be explained by simple hydration via reaction (1), and this zone should extend further into the marbles than the front in stable isotopes. However, there are no clear steps in the wollastonite content, and marbles throughout the wollastonite marbles have undergone silica metasomatism. Additionally, resetting of oxygen isotopes has occurred throughout the wollastonite marbles. These data are most consistent with fluid flow on the metre to tens of metre scale being dominantly along the wollastonite layer; the relatively sharp boundaries of the layer, and the fact that the layer runs parallel to original bedding are also probably most consistent with this conclusion.

Modal percentage wollastonite: variable fluid fluxes and intrinsic permeabilities

Given that the unmetasomatized marbles in this part of the Reynolds Range have relatively uniform calcite contents (Fig. 5), the marbles that have the highest wollastonite contents probably show the greatest progress of reaction (1A). Although the fluid flow system is not well enough defined to model fluid fluxes precisely, some idea of the relative difference in fluid fluxes recorded by and within individual samples can be made. From the above calculations it is evident that, for any given distance along a flow path, the formation of large volumes of wollastonite by metasomatism requires time-integrated fluid fluxes that

are one to two orders of magnitude higher than those required to drive reaction (1) to completion. A similar relationship is apparent from Barton *et al.* (1991, their fig. 9). If fluid flow on the scale of a thin section occurs over a similar period of time, variations in time-integrated fluid fluxes correspond to similar variations in actual fluid fluxes.

Fluid fluxes (v) are related to intrinsic permeability (K_ϕ) via Darcy's Law:

$$v = \frac{-K_\phi}{\eta} \cdot \frac{dP}{dz} \qquad \text{(iv)}$$

(e.g. deMarsily 1986), where η is the fluid viscosity, and dP/dz is the fluid pressure gradient. Hence, the difference in time-integrated fluid fluxes inferred above may reflect variations in intrinsic permeabilities of one to two orders of magnitude on the scale of a few millimetres to a few centimetres. Permeability variations of similar orders of magnitude have been proposed for calcareous rocks in other terranes (e.g. Cartwright & Oliver, 1992, 1994; Cartwright & Weaver, 1993; Cartwright, 1994). Fluid flow may have been along the grain boundaries (especially if permeabilities are enhanced by metamorphic reactions) or within microcracks (e.g. Etheridge *et al.*, 1983). Although the volume change associated with the proposed metasomatic reaction (1A) is small, there is a volume reduction of the solid phases of *c.* 22.7 cm^3/mol wollastonite produced as reaction (1) is crossed. We envisage that fluid introduced into the rock (possibly along microcracks) caused reaction (1) to proceed and created a reaction-enhanced permeability in millimetre-wide zones. These zones became channels of high fluid flux that persisted during the fluid flow event partly due to the fact that reaction (1A) does not cause a reduction in permeability. The spacing of the wollastonite-rich and wollastonite-poor zones may reflect the spacing or density of the initial microcracks.

Resetting of O and C isotope ratios in wollastonite marbles

Fluid infiltration combined with metamorphic reaction should produce distinctive $\delta^{18}O$ vs. $\delta^{13}C$ trends and a correlation between $\delta^{13}C$ and the degree of devolatilization.

$\delta^{13}C(Cc)$ vs. wt% calcite: effects of devolatilization

The trend in $\delta^{13}C(Cc)$ vs. wt% calcite in the wollastonite marbles (Fig. 6c) is similar in general form to that predicted to occur by isotopic fractionation during devolatilization (e.g. Bowman *et al.*, 1985; Valley, 1986). The marbles probably show the formation of wollastonite at the expense of calcite and quartz by reactions (1) and (1A). The predicted trend in $\delta^{13}C(Cc)$ vs. wt% calcite for devolatilization of a marble with an initial calcite content of 75% and an initial $\delta^{13}C(Cc)$ of −0.1‰ (corresponding to a typical calcite marble) by batch and Rayleigh fractionation is shown in Fig. 6(c). A value of $\Delta^{13}C(CO_2\text{-calcite})$ of 3.3 was initially used, corresponding to the isotopic fractionation at 700° C (Chacko *et al.*, 1991). Under these conditions, neither the batch nor the Raleigh fractionation trend encompasses the majority of the data and, although the marbles have evidently lost CO_2, the actual shift in $\delta^{13}C(Cc)$ is much less than predicted by the devolatilization calculations, even under batch conditions. $\Delta^{13}C(CO_2\text{-calcite})$ values vary by less than 1‰ in the 600–800° C range (Chacko *et al.*, 1991), suggesting that slight errors in the calculated temperatures of fluid infiltration cannot explain the discrepancy.

The devolatilization calculations as applied above, and in several other studies (see summaries in Valley, 1986 and Nabelek, 1991), are based on the ^{13}C fractionation between CO_2 and calcite. However, as discussed above, the Reynolds Range rocks were infiltrated by water-rich fluids. In water-rich fluids, C probably occurs occur as a variety of species other than CO_2 (e.g. HCO_3^- or H_2CO_3) that have lower ^{13}C fractionations with calcite than CO_2 (Ohmoto, 1972). At more oxidizing conditions than those at which graphite is stable, carbon speciation varies with pH with HCO_3^- becoming more dominant over H_2CO_3 at higher pH values (Ohmoto, 1972). At 250° C this results in the ^{13}C fractionations between bulk carbon species in the fluid and calcite decreasing by *c.* 5‰ between fluids with a pH of 4 and those with a pH of 9. The calculated speciation of carbon in a fluid of $X_{CO_2} = 0.2$ at 700° C and 450 MPa, using the SUPCRT92 computer program of Johnson *et al.* (1992) indicates that, for a wide range of pH values (3–12), H_2CO_3 is by far the dominant carbon species (≥95 mol% of all C). Carbon isotope fractionations between H_2CO_3 and calcite are not known at metamorphic conditions; however, the data of Ohmoto (1972), Friedman & O'Neil (1977) and Chacko *et al.* (1991) suggest that values of $\Delta^{13}C(H_2CO_3\text{-calcite})$ are less than $\Delta^{13}C(CO_2\text{-calcite})$. As shown by Fig. 6 $\delta^{13}C(Cc)$ vs. wt% calcite batch and Rayleigh devolatilization trends calculated using a $\Delta^{13}C(\Sigma C\text{-calcite})$ value of *c.* 1.0 encompass much of the Reynolds Range marble data. We suggest that this may account for the trend observed in Fig. 6. Decarbonation of calcareous rocks during fluid flow almost universally occurs in the presence of an aqueous fluid phase and the possibility that the $\Delta^{13}C(CO_2\text{-calcite})$ fractionations do not always apply to these systems is important in modelling isotopic resetting in other terranes.

$\delta^{18}O$ vs. $\delta^{13}C$: effects of infiltration combined with devolatilization

Because the volume of oxygen lost during devolatilization is small relative to carbon, the large shifts in $\delta^{18}O(Cc)$ values in the wollastonite marbles are most likely to reflect infiltration of water-rich fluids, not devolatilization. However, the trend of $\delta^{18}O(Cc)$ vs. $\delta^{13}C(Cc)$ values (Fig. 8) is unlike those predicted for fluid infiltration alone. For marbles that are infiltrated by water-rich fluids, the concentration of O in the fluid relative to the rock is much higher than the concentration of C in the fluid relative to the rock. Hence, resetting of $\delta^{18}O$ requires smaller

volumes of infiltrating fluid than are required to reset $\delta^{13}C$ values. Both advection–dispersion and one-box models predict that the infiltration of water-rich fluids into carbonates should produce L-shaped trends on $\delta^{18}O(Cc)$ vs. $\delta^{13}C(Cc)$ diagrams (e.g. Baumgartner & Rumble, 1988), as shown by curve A in Fig. 8(a). Changing C contents during infiltration as devolatilization proceeds will significantly modify such curves; however, for a fluid of $X_{CO_2} < 0.2$, rocks with ≥24wt% calcite should show a greater relative resetting of oxygen isotopic ratios than carbon isotopic ratios. However, this is not reflected in Fig. 8, in which $\delta^{18}O(Cc)$ vs. $\delta^{13}C(Cc)$ defines a near linear trend. Similar linear trends have been documented from metasomatized marbles in other terranes (e.g. Jamtveit *et al.*, 1992, their fig. 9).

If fluid flow were perfectly channelled on a millimetre scale, the trend in $\delta^{18}O(Cc)$ vs. $\delta^{13}C(Cc)$ values might result from mechanical mixing of unreset and reset zones during sampling (Fig. 8b). The alternation of wollastonite-rich and wollastonite-poor zones implies fluid focusing on this scale; however, such perfect channelling is unlikely. The observed $\delta^{18}O(Cc)$ vs. $\delta^{13}C(Cc)$ trend is also close to that expected to result from diffusion (Baumgartner & Rumble, 1988 their fig. 1), as shown by curve D in Fig. 8(a). As noted above, diffusion of stable isotopes over distances of more than a few centimetres to a few metres is unlikely in metamorphic environments, and in general X_{H_2O} values are not raised sufficiently by diffusion to stabilize wollastonite (Cartwright & Valley, 1991). Hence, diffusion may not seem to be an important process in the formation of the wollastonite marbles. However, a possible consequence of focused fluid flow (such as that documented here) is to allow transverse dispersion (either molecular diffusion and/or kinematic dispersion) between the zones of high and low fluid fluxes (e.g. as inferred by Jamtveit *et al.*, 1992; Cartwright, 1994). It is unlikely that this model can explain the isotopic trends, as fluid infiltration would still be expected to produce L-shaped $\delta^{18}O(Cc)$ vs. $\delta^{13}C(Cc)$ profiles similar to those discussed above. Hence, unless transverse dispersion occurred between perfectly reset and unreset rocks, dispersion would result in a spread of isotopic ratios between the infiltration and dispersion curves (shaded area in Fig. 8b).

Given the evidence for devolatilization discussed above, we consider that the distinct $\delta^{18}O(Cc)$ vs. $\delta^{13}C(Cc)$ trend results from fluid infiltration combined with devolatilization. The shift in $\delta^{18}O$ values is probably dominantly due to infiltration, whereas, as discussed above, the shift in $\delta^{13}C$ values probably has a much higher contribution from devolatilization. The isotopic ratios of the grandite-rich zones are the most reset, and probably approached isotopic equilibrium with the incoming fluid.

Fluid–rock interaction in marl layers

The marl layers within the wollastonite marbles do not contain wollastonite and therefore have not been infiltrated by large volumes of water-rich fluids. However, these marls are considerably coarser grained than their counterparts in the calcite marbles and have slightly lower $\delta^{13}C(Cc)$ and $\delta^{18}O(Cc)$ values. Both of these features plausibly reflect at least limited fluid–rock interaction. Unlike fluid infiltration, fluid-hosted diffusion would almost certainly not lower X_{CO_2} values sufficiently to stabilize wollastonite (e.g. Cartwright & Valley, 1991) but would potentially reset the stable isotope ratios and cause coarsening due to recrystallization. The convergence of $\delta^{18}O(Cc)$ values between the marble and the marl noted in sample 9235-368 (Fig. 9) is also suggestive of isotopic diffusion.

Origin and timing of the grandite-rich zones

As discussed above, these zones are confined to the junction between the marl and marble layers in the wollastonite marbles. The garnet locally encloses wollastonite in the marble layers, suggesting that the formation of these layers outlasted the formation of wollastonite. Because the layers are confined to the wollastonite marbles, it is likely that they are also products of fluid infiltration. The garnet grains that occur in these zones are Fe rich, whereas all minerals in the surrounding marl and marbles are Mg–Ca dominated (Table 2). This makes it highly unlikely that simple diffusion between the marble and the marl (for instance as inferred by Buick *et al.*, 1993, for the formation of reaction zones in Rauer Group marbles) can explain the mineral assemblages of these grandite-rich zones. These layers may represent zones of intense fluid infiltration where Fe metasomatism and more complete decarbonation has occurred. Such major chemical changes suggest that these zones may record the highest fluid fluxes, and the fact that these zones show the highest degree of isotopic resetting (Fig. 5) is consistent with this interpretation. Similar, but much thicker, grandite-rich zones are recognized in marbles of the Lower Calcsilicate unit of the Reynolds Range Group and are interpreted in a similar fashion, although in that unit the layers are folded by $F2_2$ folds, and fluid flow accompanied $M2_1$ contact metamorphism (Buick *et al.*, 1994a).

Pattern of fluid infiltration and origin of fluids

Fluid flow was channelled on all scales. The wollastonite marbles form a 40–45-m-wide strike-parallel zone that represents a channel for along-strike fluid flow. The widths of wollastonite marbles and the associated orthoamphibole-bearing metapsammite rocks vary markedly (Fig. 2). The zones where wollastonite and orthoamphibole are most abundant probably experienced extensive fluid infiltration, and we interpret these zones as mapping out the metre- to tens-of-metre-scale pattern of metamorphic fluid flow. Fluids were also strongly channelled on a small scale. The marls have similar mineral assemblages both within and outside the wollastonite zones and have probably not been infiltrated by significant volumes of fluid. The variable wollastonite contents of the marbles are best explained by variable

progress of the mineralogical and metasomatic reactions (1) and (1A) that is due to different degrees of fluid infiltration on a millimetre to centimetre scale. As discussed above, the grandite-rich zones in the wollastonite marbles may be a further expression of fluid channelling. Late fluid flow in these rocks includes the formation of centimetre-wide calcite and garnet veins, and the epidote in the marl layers. This late veining may reflect a change from fluid flow through the bulk of the rocks to fluids being hosted in discrete mesoscopic fractures. Similar transitions have been noted in metasomatized calcsilicate rocks in other metamorphic terranes (e.g. Cartwright & Weaver, 1993; Cartwright & Oliver, 1994)

The lowest calcite $\delta^{18}O(Cc)$ and $\delta^{13}C(Cc)$ values recorded from the wollastonite marbles are approximately 11‰ and −5‰, respectively; if the grandite-rich zones are included, the lowest values are approximately 10‰ and −7‰, respectively. As discussed above, these rocks probably approached isotopic equilibrium with the infiltrating fluid. These isotopic values are close to those of calcite in equilibrium with fluids derived from 'typical' granitic bodies at high temperatures (e.g. Sheppard, 1986). As noted above, suites of pegmatites were intruded during the later stages of $M2_2$ that have $\delta^{18}O(Qtz)$ values of 11.3–13.5‰. At 700° C $\Delta^{18}O(Qtz–Cc)$ values are *c.* 0.4‰. Hence, calcite in isotopic equilibrium with a fluid derived from the pegmatites would be expected to have a $\delta^{18}O$ in the range 11–13‰, which is close to the lowest $\delta^{18}O$ values in the wollastonite marbles. We therefore suggest that the aluminous pegmatites were the source of the fluids. The pegmatites were probably derived from partial melts that formed during granulite facies metamorphism, and crystallization of the melts during cooling would have produced fluids, as has been proposed in other high-grade metamorphic terranes (e.g. Corbett & Phillips, 1981; Cartwright, 1988). The fluids may have entered the rocks via the garnet + quartz veins that cut the marbles in this part of the Reynolds Range. The two calcite marble samples with slightly lower $\delta^{18}O$ values possibly record a minor component of across-strike flow 'leaking' out of the main channels. Fluids in equilibrium with the calcite marbles must have had an X_{CO_2} of ≥0.3; hence, fluid infiltration would potentially reset both oxygen and carbon isotope ratios, and these samples do have slightly lower $\delta^{13}C$ values (Table 3a). The fluids may represent those that have had their X_{CO_2} increased by metamorphic reaction within the wollastonite marbles.

Despite the abundance of fluid within the wollastonite marbles, isotopic heterogeneities of several permil are preserved over distances of a few millimetres. As discussed above, in other terranes, diffusion of oxygen isotopes during metamorphism over distances of several centimetres to a few metres has been inferred. The preservation of steep isotopic gradients in a fluid-dominated system may be evidence of very rapid fluid infiltration during which there was little time for significant diffusion. Alternatively, it may reflect the palaeopermeability structure of the rocks. If the marbles were relatively impermeable, except where cut by microfractures, diffusion or fluid flow away from the fractures into the bulk of the rock would be limited.

The formation of rocks with alternating wollastonite-rich and wollastonite-poor zones as inferred in this study also probably depends on the volume of fluid. There must obviously be sufficient fluid to enable the transport of silica; however, very large volumes of fluids (such as may be present in some contact metamorphic skarn systems) would tend to cause more pervasive metasomatism. The rocks from this study may thus reflect a channelled fluid flow system with 'moderate' volumes of fluid. This conclusion is in agreement with the general geological setting of late $M2_2$ fluid flow in the Reynolds Range Group, where fluids were derived from pegmatites that are a relatively minor component of the terrane. Additionally, in contrast to many examples of metamorphic fluid flow that homogenize stable isotope or activity gradients, the fluid flow in the Upper Calcsilicate unit produced a very heterogeneous pattern of mineralogical and isotopic resetting.

CONCLUSIONS

Wollastonite marbles in the Reynolds Range are important for documenting the patterns and conditions of late-regional metamorphic fluid flow. The simple observation of the distribution and modal volume of wollastonite allows constraints to be placed on the direction of fluid flow and the permeability structure of the rocks. Fluid channelling is evident at all scales from hundreds of metres to millimetres, and was largely parallel to strike. Wollastonite marbles are commonly formed by contact-metamorphic fluid flow, and less commonly (as in this area) by fluid flow during regional metamorphism. In certain terranes (e.g. massive wollastonite–calcite rocks in the Adirondack Mountains; Valley *et al.*, 1990; Gerdes & Valley, 1994) the volumes of wollastonite formed are too high to be explained by the simple hydration of calcite and quartz in typical marble precursors. In these cases additional metasomatism is almost certainly required to produce the observed volumes of wollastonite. Recognition of the reactions that form wollastonite is important for calculating fluid fluxes and intrinsic permeabilities, as metasomatic reactions imply the involvement of far greater volumes of fluid than simple hydration.

ACKNOWLEDGEMENTS

For help with the analyses we thank A. Kos and R. Smackman (stable isotopes), and D. Sewell (electron microprobe). We are also indebted to D. Gelt for drafting some of the figures and to M. Wallace for use of the cathodoluminescope. This research was supported by ARC grants A39030662 and A39231141 (to I.C.), and I.C. gratefully acknowledges receipt of an ARC Queen Elizabeth II fellowship. I.S.B. was supported by ARC grant A38930485 to R. Powell and C. Wilson and an ARC research fellowship. Helpful comments by N. D. J. Cook,

A. S. Andrew and R. H. Vernon improved the clarity of the manuscript.

REFERENCES

Barton, M.D., Ilchik, R.P. & Marikos, M.A. 1991. Metasomatism. In: *Contact Metamorphism* (ed. Kerrick D.M.), *Mineralogical Society of America Reviews in Mineralogy*, **26,** 321–345.

Baumgartner, L.P. & Ferry J.M. 1991. A model for coupled fluid-flow and mixed-volatile mineral reactions with applications to regional metamorphism. *Contributions to Mineralogy and Petrology*, **106,** 273–285.

Baumgartner, L.P. & Rumble, D.I. 1988. Transport of stable isotopes: 1: development of a kinetic continuum theory for stable isotope transport. *Contributions to Mineralogy and Petrology*, **98,** 417–430

Bear, J. 1972. *Dynamics of Fluid Flow in Porous Media*. Dover Publications, New York.

Bickle, M.J. & Baker, J. 1990. Advective–diffusive transport of isotopic fronts: an example from Naxos, Greece. *Earth and Planetary Science Letters*, **97,** 78–93.

Bickle, M.J. & McKenzie, D.M. 1987. The transport of heat and matter by fluids during metamorphism. *Contributions to Mineralogy and Petrology*, **95,** 384–392.

Black, L.P., Shaw, R.D. & Stewart, A.J. 1983. Rb–Sr geochronology of Proterozoic events in the Arunta Inlier, central Australia. *Bureau of Mineral Resources Journal of Australian Geology and Geophysics*, **8,** 129–138.

Bowman, M.J., O'Neil, J.R. & Essene, E.J. 1985. Contact skarn formation at Elkhorn, Montana. II: Origin and evolution of C-O-H skarn fluids. *American Journal of Science*, **285,** 621–660.

Bowman, M.J. & Willet, S.D. 1991. Spatial patterns of oxygen isotope exchange during one-dimensional fluid infiltration. *Geophysics Research Letters*, **18,** 971–974.

Buick, I.S. & Cartwright, I. 1994. The significance of early scapolite in greenschist facies marbles from the Reynolds Range Group, central Australia. *Journal of the Geological Society of London*, **151,** 803–812.

Buick, I.S., Harley, S.L. & Cartwright, I. 1993. Granulite facies metasomatism: zoned calc-silicate boudins from the Rauer Group, East Antarctica. *Contributions to Mineralogy and Petrology*, **113,** 557–571.

Buick, I.S., Cartwright, I., Hand, M. & Powell, R. 1994a. Evidence for pre-regional metamorphic fluid infiltration of the Lower Calcsilicate Unit, Reynolds Range Group (central Australia). *Journal of Metamorphic Geology*, **12,** 789–810.

Buick, I.S., Harley, S.L., Cartwright, I. & Mattey, D. 1994b. Stable isotopic signatures of superposed fluid events in granulite facies marbles of the Rauer Group, East Antarctica. *Journal of Metamorphic Geology*, **12,** 285–300.

Cartwright, I. 1988. Melt crystallization, pegmatite intrusion and the Inverian retrogression of the Scourian complex of NW Scotland. *Journal of Metamorphic Geology*, **6,** 77–93.

Cartwright, I. 1994. The two-dimensional pattern of metamorphic fluid flow at Mary Kathleen, Australia: fluid focusing, transverse dispersion, and implications for modeling fluid flow. *American Mineralogist*, **79,** 526–535.

Cartwright, I. & Oliver, N.H.S. 1992. The direction of fluid flow during contact metamorphism in the Burstall granite contact aureole. *Journal of the Geological Society of London*, **149,** 693–696.

Cartwright, I. & Oliver, N.H.S. 1994, Fluid flow during contact metamorphism: Mary Kathleen, Queensland, Australia. *Journal of Petrology*, in press.

Cartwright, I. & Valley, J.W. 1991. Steep oxygen-isotope gradients at marble–metagranite contacts in the northwest Adirondack Mountains, New York, USA: products of fluid-hosted diffusion. *Earth and Planetary Science Letters*, **107,** 148–163.

Cartwright, I. & Weaver, T.R. 1993. Metamorphic fluid flow at Stephen Cross Quarry, Québec: Stable isotopic and petrological data. *Contributions to Mineralogy and Petrology*, **113,** 533–544.

Chacko, T., Mayeda, T.K., Clayton, R.N. & Goldsmith, J.R. 1991. Oxygen and carbon fractionations between CO_2 and calcite. *Geochimica et Cosmochimica Acta*, **55,** 2867–2882.

Chamberlain, C.P., Ferry, J.M. & Rumble, D.I. 1990. The effect of net-transfer reactions on the isotopic composition of minerals. *Contributions to Mineralogy and Petrology*, **105,** 322–336.

Clayton, R. & Mayeda, T.K. 1963. The use of bromine pentafluoride in the extraction of oxygen from oxides and silicates for isotopic analysis. *Geochimica et Cosmochimica Acta*, **27,** 43–52.

Clarke, G.L., Collins, W.J. & Vernon, R.H. 1990. Successive early Proterozoic deformation and metamorphic events in the Anmatjira Range, central Australia. *Journal of Metamorphic Geology*, **8,** 65–88.

Clarke, G.L. & Powell, R. 1991. Proterozoic granulite facies metamorphism in the southeastern Reynolds Range, central Australia: context, *P–T* path and overprinting relationships. *Journal of Metamorphic Geology*, **9,** 267–281.

Clayton, R.N., Goldsmith, J.R. & Mayeda, T.K. 1989. Oxygen isotope fractionation in quartz, albite, anorthite, and calcite. *Geochimica et Cosmochimica Acta*, **53,** 725–733

Corbett, G J. & Phillips, G.N. 1981. Retrograde metamorphism of a high grade terrain: The Willyama complex, Broken Hill, Australia. *Lithos*, **14,** 59–79.

deMarsily, G. 1986. *Quantitative Hydrogeology*. Academic Press, San Diego.

Dipple, G.M. & Ferry, J.M. 1992. Fluid flow and stable isotopic alteration in rocks at elevated temperatures with applications to metamorphism. *Geochimica et Cosmochimica Acta*, **56,** 3539–3550.

Dirks, P.H.G.M. 1990. Intertidal and subtidal sedimentation during a mid-Proterozoic marine transgression, Reynolds Range Group, Arunta Block, central Australia. *Australian Journal of Earth Sciences*, **37,** 409–422.

Dirks, P.H.G.M. & Wilson, C.J.L. 1990. The geological evolution of the Reynolds Range, central Australia: evidence for three distinct structural-metamorphic cycles. *Journal of Structural Geology*, **12,** 651–665.

Dirks, P.H.G.M., Hand, M. & Powell, R. 1991. The *P–T* deformation path for a mid-Proterozoic, low-pressure terrane: the Reynolds Range, central Australia. *Journal of Metamorphic Geology*, **9,** 641–661.

Engi, M. & Wersin, P. 1987. Derivation and application of a solid solution model for calcic garnet. Schweizerisches *Mineralogisches und Petrographisches Mitteilungen*, **67,** 53–73.

Etheridge, M.A., Wall, V.J. & Vernon, R.H. 1983. The role of the fluid phase during regional metamorphism and deformation. *Journal of Metamorphic Geology*, **1,** 205–226.

Ferry, J.M. 1991. Dehydration and decarbonation reactions as a record of fluid infiltration. In: *Contact Metamorphism* (ed. Kerrick, D.M.), *Mineralogical Society of America Reviews in Mineralogy*, **26,** 351–393.

Ferry, J.M. & Dipple, G.M. 1991. Fluid flow, mineral reactions, and metasomatism. *Geology*, **19,** 211–214

Ferry, J.M. & Dipple, G.M. 1992. Models for coupled fluid flow, mineral reaction, and isotopic alteration during contact metamorphism: the Notch Peak aureole, Utah. *American Mineralogist*, **77,** 577–591.

Friedman, I. & O'Neil, J.R. 1977. Compilation of stable isotope fractionation factors of geochemical interest. In: *Data of Geochemistry, 6th edn* (ed. Fleischer, M). *United States Geological Survey Professional Paper*, **440-KK**.

Ganor, J., Matthews, A. & Paldor, N. 1989. Constraints on effective diffusivity during oxygen isotope exchange at a marble-schist contact, Sifnos (Cyclades), Greece. *Earth and Planetary Science Letters*, **94,** 208–216.

Gerdes, M.L. & Valley, J.W. 1994. Fluid flow and mass transport at the Valentine wollastonite deposit, Adirondack Mountains,

New York State. *Journal of Meramorphic Geology*, **12,** 589–608.

Hand, M., Dirks, P.H.G.M., Powell, R & Buick, I.S. 1992. How well established is isobaric cooling in Proterozoic orogenic belts? An example from the Arunta inlier, central Australia. *Geology*, **20,** 649–652.

Harley, S.L. & Buick, I.S. 1992. Wollastonite-scapolite assemblages as indicators of granulite pressure-temperature-time histories: the Rauer Group, East Antarctica. *Journal of Petrology*, **33,** 693–728.

Holland, T.J.B. & Powell, R. 1990. An enlarged and updated internally consistent thermodynamic dataset with uncertainties and correlations: the system K_2O–Na_2O–CaO–MgO–MnO–FeO–Fe_2O_3–Al_2O_3–TiO_2–SiO_2–C–H_2–O_2. *Journal of Metamorphic Geology*, **8,** 89–124.

Jamtveit, B., Grorud, H.F. & Bucher-Nurminen, K. 1992. Contact metamorphism of layered carbonate–shale sequences in the Oslo Rift. II: Migration of isotopic and reaction fronts around cooling plutons. *Earth and Planetary Science Letters*, **114,** 131–148.

Johnson, J.W., Delkers, E.H. & Helgeson. H.C. 1992. SUPCRT92: A software package for calculating the standard molal thermodynamic properties of minerals, gases, aqueous species, and reactions from 1 to 5000bars and 0–1000° C. *Computers and Geosciences*, **18,** 899–947.

Matthews, A, Goldsmith, J.R. & Clayton, R.M. 1983. Oxygen isotope fractionations involving pyroxenes and the calibration of mineral pair geothermometers. *Geochimica et Cosmochimica Acta*, **47,** 631–647.

McCrea, J.M. 1950. On the isotope chemistry of carbonates and a paleotemperature scale. *Journal of Chemical Physics*, **18,** 849–57.

Myers, J. & Eugster, H.P. 1983. The system Fe–Si–O: oxygen buffer calibrations to 1500K. *Contributions to Mineralogy and Petrology*, **82,** 75–90.

Nabelek, P.I. 1991. Stable isotope monitors. In: *Contact Metamorphism* (ed. Kerrick, D.M.), *Mineralogical Society of America Reviews in Mineralogy*, **26,** 395–436.

Nabelek, P.I., Labotka, T.C. & Russ-Nabelek, C. 1992. Stable isotope evidence for the role of diffusion, infiltration, and local structure on contact metamorphism of calc-silicate rocks at Notch Peak, Utah. *Journal of Petrology*, **33,** 557–83.

Norton, D. & Knight, J. 1977. Transport phenomena in hydrothermal systems: Cooling plutons. *American Journal of Science*, **277,** 913–36.

Ohmoto, H. 1972, Systematics of sulfur and carbon isotopes in hydrothermal ore deposits. *Economic Geology*, **67,** 551–579.

Powell, R. & Holland, T.J.B. 1989. An internally consistent thermodynamic dataset with uncertainties and correlations: 3: Applications to geobarometry, worked examples and a computer program. *Journal of Metamorphic Geology*, **6,** 173–204.

Robie, R.A., Hemingway, B.S. & Fisher, J.R. 1978. Thermodynamic properties of minerals and related substances at 298.15 K and 1 bar (10^5 pascals) pressure and higher temperatures. *United States Geological Survey Bulletin*, **1452.**

Stewart, A.J., Offe, L.A., Glikson, A.J., Warren, R.G. & Black, L.P. 1980.Geology of the northern Arunta Block, Northern Territory. Australian Bureau of Mineral Resources, *Geology and Geophysics Record*, **1980/83.**

Sheppard, S.M.F. 1986. Characterisation and isotopic variations in natural waters. In: *Stable Isotopes in High Temperature Geological Processes* (eds Valley, J.W., Taylor, H.P. & O'Neil, J.R), *Mineralogical Society of America Reviews in Mineralogy*, **16,** 165–184.

Tracy, R.J. & Frost, B.R. 1991. Phase equilibria and thermobarometry of calcareous, ultramafic and mafic rocks, and iron formations. In: *Contact Metamorphism* (ed. Kerrick, D.M.), *Mineralogical Society of America Reviews in Mineralogy*, **26,** 207–290.

Todd, C.S. & Evans, B.W. 1993. Limited fluid-rock interaction at marble-gneiss contacts during Cretaceous granulite-facies metamorphism, Seward Peninsula, Alaska. *Contributions to Mineralogy and Petrology*, **114,** 27–41.

Valley, J.W. 1986. Stable isotope geochemistry of metamorphic rocks. In: *Stable Isotopes in High Temperature Geological Processes* (eds Valley, J.W., Taylor, H.P. & O'Neil, J.R), *Mineralogical Society of America Reviews in Mineralogy*, **16,** 445–490.

Valley, J.W., Bohlen, S.R., Essene, E.J. & Lamb, W. 1990. Metamorphism in the Adirondacks: II The role of fluids. *Journal of Petrology*, **31,** 555–596.

Vry, J.K. & Cartwright, I. 1993, Sapphirine-kornerupine rocks from the Reynolds Range, central Australia: constraints on the uplift history of a Proterozoic low pressure terrane. *Contributions to Mineralogy and Petrology*, **116,** 78–91.

Warren, R.G. & Stewart, A.J. 1988. Isobaric cooling of Proterozoic high-temperature metamorphites in the northern Arunta Block, central Australia. *Precambrian Research*, **40/41,** 175–198.

Yardley, B.W.D. & Lloyd. G.E., 1989. An application of cathodoluminescence microscopy to the study of textures and reactions in high-grade marbles from Connemara, Ireland. *Geological Magazine*, **126,** 333–337.

Zheng, Y-F. 1993. Calculation of oxygen isotope fractionation in hydroxyl-bearing silicates. *Earth and Planetary Science Letters*, **120,** 247–263.

Received 15 March 1994; revision accepted 27 September 1994.